

The Pennsylvania State University

The Graduate School

**UPDATED SUBLATTICE MODELS OF TOPOLOGICALLY CLOSE PACKED PHASES  
WITH A REVISED PHASE DESCRIPTION OF  $\sigma$  PHASE**

A Thesis in

Material Science and Engineering

by

Matthew Feurer

© 2019 Matthew Feurer

Submitted in Partial Fulfillment  
of the Requirements  
for the Degree of

Master of Science

December 2019

The thesis of Matthew Feurer was reviewed and approved\* by the following:

Zi-Kui Liu  
Distinguished Professor of Materials Science and Engineering  
Thesis Co-Advisor

Allison Beese  
Associate Professor of Materials Science and Engineering  
Associate Professor of Mechanical Engineering  
Thesis Co-Advisor

Ismaila Dabo  
Associate Professor of Materials Science and Engineering

Susan Sinnott  
Professor, Materials Science and Engineering and Chemistry  
Department Head, Materials Science and Engineering

\*Signatures are on file in the Graduate School

## ABSTRACT

Frank Kasper Topologically Close Packed (TCP) phases are a wide class of intermetallic phases known to occur in a wide variety of metallic alloy systems, often occurring where elements have different radii and electronic properties. They are known as detrimental phases in alloys, occurring in many of the most technologically significant alloys. The formation of these phases often leading to poor mechanical properties and detriment to corrosion properties.

There has been great progress since Kasper in understanding the structure and occurrence of TCP phases, however modeling of these phases has still been a difficult task using the CALculation of PHase Diagram (CALPHAD) method. High solubility, magnetism, and complex structure all provide additional challenges in modeling these phases within the context of CALPHAD. Such challenges have led to the adoption of multiple models for describing a single phase, and has been an impediment to the development of higher order databases.

In many situations it is the choice of the modeler to either retain compatibility or to increase physical accuracy. In the following work the criteria for sublattice models will be discussed and identified. Following this the sublattice models of common TCP phases will be reviewed with the previously identified criteria. Development of an updated sublattice model with increased physical accuracy will be demonstrated for the sigma phase. Discussion of how High throughput methods can be incorporated into the creation of CALPHAD models (density functional theory, optimization and machine learning methods) will also be included. Finally revised sublattice models will be presented with the intent for future modelers to coordinate their efforts between disparate and higher order systems.

## TABLE OF CONTENTS

LIST OF FIGURES .....	vi
LIST OF TABLES .....	vii
ACKNOWLEDGEMENTS .....	viii
Chapter 1 Introduction .....	1
Background .....	1
Frank Kasper TCP Phases .....	1
Need for improved models for complex solids .....	2
Scope .....	4
Chapter 2 Theory .....	6
Criteria for sublattice models in complex solids .....	6
Wyckoff positions .....	6
Coordination Number .....	7
Experimental Data .....	8
Physical Accuracy and the Tradeoff Therein .....	12
Sublattice models in complex solids .....	13
Laves Phases .....	13
$\mu$ phase .....	16
$\chi$ Phase .....	19
$\delta$ Phase .....	21
R Phase .....	22
Demonstration of improved model for $\sigma$ phase .....	23
Chapter 3 Methods .....	26
High throughput DFT with DFTTK .....	26
Overview .....	26
Structure Relaxation .....	28
E-V Curve .....	29
Debye Model .....	30
Checking and Validation Steps .....	31
High throughput CALPHAD modeling Espei .....	33
Overview of software with capabilities .....	33
Selection of model parameters .....	33
Optimization to Phase Equilibria .....	34
Chapter 4 Analysis .....	35
DFT calculations for $\sigma$ phase .....	35
Creation of the $\sigma$ phase thermodynamic database .....	40

Chapter 5 Discussion .....	45
Revised sublattice models of TCP phases.....	45
Chapter 6 Conclusion.....	49
REFERENCES .....	51

## LIST OF FIGURES

Figure 1-1: Homogeneity ranges for TCP phases.....	1
Figure 1-2: Embrittlement in ferritic austenitic duplex steel. ....	2
Figure 2-1: Gibbs energy for generic 2 sublattice system.....	10
Figure 2-2: Connection between energy surface and site occupancies.....	11
Figure 2-3: Crystallographic info Laves C15. ....	14
Figure 2-4: Crystallographic info Laves C14. ....	15
Figure 2-5: Crystallographic info Laves C36. ....	16
Figure 2-6: Crystallographic info mu-phase. ....	17
Figure 2-7: Site occupancies in the mu-phase. ....	19
Figure 2-8: Crystallographic info $\chi$ -phase. ....	20
Figure 2-9: Site occupancies in the $\chi$ -phase.....	21
Figure 2-10: Crystallographic info $\delta$ -phase .....	22
Figure 2-11: Crystallographic info r-phase.....	23
Figure 2-12: Crystallographic info $\sigma$ -phase. ....	24
Figure 3-1: DFTTK workflow. ....	27
Figure 4-1: Magnetization-energy curve.....	36
Figure 4-2: Heat capacity of the $\sigma$ -phase. ....	39
Figure 4-3: Calculated site occupancies of the Fe-Cr $\sigma$ -phase. ....	41
Figure 4-4: Site occupancies for $\sigma$ phase in Fe-Ni & Ni-Cr. ....	42
Figure 4-5: Plotted Enthalpy/Gibbs Energy.....	43
Figure 4-6: Phase diagram. ....	45

## LIST OF TABLES

Table 4-1: Magnetic moments comparison at fixed magnetization. ....	36
Table 4-2: Endmember energies for $\sigma$ compared with literature. ....	38
Table 4-3: Poisson ratios from elastic calculations. ....	40
Table 5-1: Summary of more physically accurate sublattice models. ....	49

## ACKNOWLEDGEMENTS

This dissertation could not have been accomplished without the help and support of my advisors Dr. Zi-Kui Liu and Dr. Allison Beese. They have helped me with many aspects. Dr. Liu for his deep knowledge in thermodynamics of materials inspires me a lot, which now becomes an important part of my knowledge. Dr. Beese for her depth of knowledge in Additive manufacturing, mechanical properties, and process property relations which has given me great intuition as I move forward in my career. In addition to my advisors, I would like to thank the rest of my committee, Dr. Ismaila Dabo for his time, encouragements and suggestions while serving on my dissertation committee. I would like to thank many of my colleagues in the Phases Research Lab for their help and discussions.

The financial support from the Office of Naval Research under contract N00014-17-S-F003 is greatly acknowledged. Any opinions, findings, and conclusions or recommendations expressed in this material are those of the author and do not necessarily reflect the views of the Office of Naval Research. First-principles calculations also partially used the Extreme Science and Engineering Discovery Environment (XSEDE), which is supported by National Science Foundation Grant **No. ACI-1053575**, and were partially carried out on the ACI clusters at the Pennsylvania State University supported by the Materials Simulation Center and the Institute for CyberScience.



## Chapter 1

### Introduction

#### Background

#### Frank Kasper TCP Phases

Frank Kasper Topologically Close Packed (TCP) phases are a wide class of intermetallic phases known to occur in a wide variety of metallic alloy systems, often occurring where elements have different radii and electronic properties. In fact it was suggested by Kasper that atomic arrangements in intermetallic phases are determined by radii completing close packing requirements<sup>1</sup>. These phases are ubiquitous for their complex structures and high solubility (See Figure 1-1).

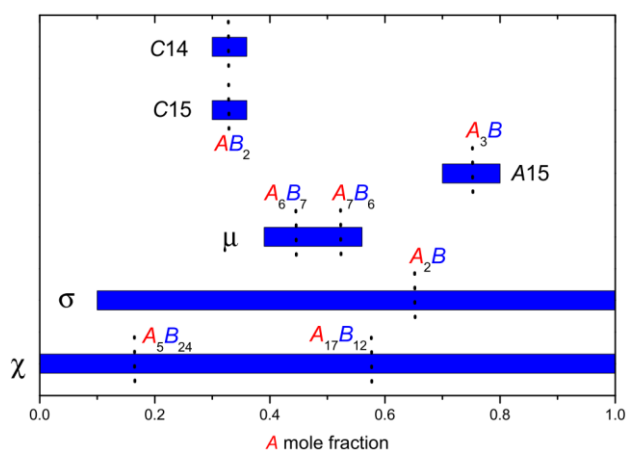


Figure 1-1: Solubility ranges of select TCP phases with ideal stoichiometry marked<sup>65</sup>

TCP phases are of great interest due to their formation in many technologically important alloy systems. The brittle nature and high solubility in these structures have led to them being

dubbed detrimental phases; best known for causing significant deterioration of mechanical properties in highly alloyed steels, illustrated in Figure 1-2<sup>2</sup>. For this reason it is often the goal to model their precipitation and subsequently avoid their occurrence. Modeling of TCP phases and their stability has become one of the primary goals of the CALPHAD community.

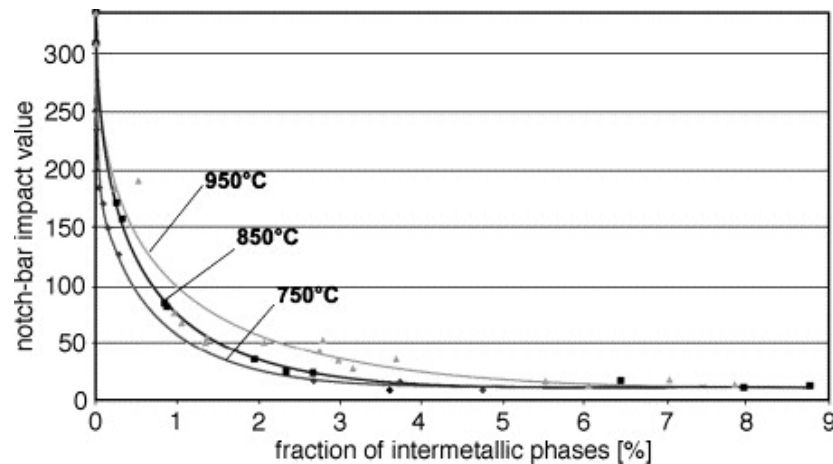


Figure 1-2: Precipitation of  $\sigma$ -Phase in highly alloyed steels. Data above showing embrittlement of ferritic austenitic duplex steel<sup>2</sup>

There has been great progress since Kasper in understanding the structure and occurrence of TCP phases, however modeling of these phases has still been a difficult task using the CALPHAD method. In the following paragraphs these challenges will be outlined so that the task of modeling them might be better understood.

### Need for improved models for complex solids

Often it is the choice of the modeler to select the appropriate sublattice models for describing the system in question under the given constraints. In this way multiple models for a phase can be employed with great success despite describing the same structure. While this practice might be more than adequate for describing a single binary or ternary system, it often leads to issues when developing multicomponent databases. To be explicit, it is often the situation that sublattice

models between databases are incompatible. This is unfortunate as there are cases where it has led to the adoption of suboptimal sublattice models just to retain compatibility in making larger databases. This is no small issue as one of the major thrusts of the CALPHAD community is in building higher order databases.

The large solubility found in TCP phases presents an additional challenge to the CALPHAD community as current models don't accurately describe the site occupancies found in these structures. There have been many recent efforts to update (but not restructure) sublattice models to include more solubility and therefore make them more applicable to a larger number of systems. Historical approaches to include solubility in the absence of definitive experimental data has been to model one sublattice as component A, one as component B, and to include mixing on a third sublattice. The decision on which of these sites to include solubility on has been somewhat arbitrary and often creating a model that spans the entire observed solubility range was the primary concern. This often leads to models which pair sites having dissimilar solubility, leading to models which cannot reproduce experimentally observed site occupancies.

Even among models which adequately reproduce site occupancies, metastable states are often not considered. For calculations where only stability is needed (such as producing phase diagrams) this works perfectly well. As stated earlier it is often the goal when modeling tcp phases to avoid their formation in real processes which occur outside of equilibrium. Inclusion of metastable and even unstable states into a model will aid in these predictions. Additionally such models can provide better extrapolation to higher order systems. Such knowledge of non equilibrium states is crucial to development of high entropy alloys and functionally graded materials where wide compositions spaces are often explored.

At this point it should be obvious that if multiple incompatible descriptions can be used successfully, then incorrect phase descriptions can be made to give correct results. This is a problem that is not unique to TCP phases and is an issue intrinsic to the CALPHAD method in

general. There are two ways in which an incorrect phase description can give correct results, in so much as phase diagrams and equilibria are concerned.

The first is that because the energies in CALPHAD are relative it is necessary to define a reference state for the system, so that they may be compared. Phase equilibria between phases are dependent only on the relative energies and not their absolute values. It is because of this that incorrect energies in one phase in the system can be propagated to others in optimizing the database. The result is a phase description in which the equilibria match in so much as parameters have been optimized to do so, but where site properties or others do not. It is for this reason that experimental validation and first principle calculations of thermodynamic properties pertaining to individual phases is critical to producing a database that extrapolates well to higher order systems.

A second way that incorrect phase descriptions, in particular incorrect sublattice models, can produce correct equilibria is in the optimization of the phases themselves. Given enough degrees of freedom in optimizing parameters their energies can be made to give energies on the convex hull. On other words parameters can be made to give results for the equilibrium structure rather than the structure they represent. This is an incorrect way to represent equilibrium as it becomes impossible to correctly represent metastable states. The analogy has often been made between equilibrium and the surface of a lake. Where in the surface of the lake obscures the lakes' bed (metastable/unstable states). In this case any given parameter can be fit to give the value of this energy surface. In doing so you lose the ability to rigorously describe anything below this surface. Metastable states become important for understanding and predicting phase transitions under realistic conditions, and extrapolating to higher order.

## Scope

The following work will explore common topologically close packed structures which form in metallic systems, often of great industrial significance. More specifically relevant experimental findings and historical descriptions used in CALPHAD for representing these phases will be reviewed so that the current method for modeling these phases can be assessed. In this way we hope to better understand the crystallography present. In the following chapters a criteria for developing sublattice models will then be proposed and applied to the aforementioned phases. To better match the physical structure to models, solubility and ordering will be considered. Finally, it will be demonstrated how first principles calculations can be integrated into this approach in an efficient high throughput manor to build more physical sublattice models. Demonstration of this methodology will be performed on the sigma phase.

## **Chapter 2**

### **Theory**

#### **Criteria for sublattice models in complex solids**

To develop better sublattice models for TCP phases and propose a criteria for modeling them it is first and foremost important to understand what is intended to be captured in a sublattice model. A sublattice model within the context of CALPHAD is conceptually very simple. It is a way of representing a given phase in a system as a combination of lattices. Each site in the sublattice should possess the same properties and thus be grouped. For as simple as this is it can be a daunting task to perform. Selecting how and when to combine sublattices and which constituents sit on a given site is not trivial. In the absence of experimental results such choice often comes down to the expertise of the modeler, what their goals ultimately are, and what is computationally tractable. Ideally a sublattice model can capture the same crystal structure experimentally observed, both in sites and occupation, and for this reason crystallography is often the first thing that should be considered when selecting/developing a model. This leads to the first criterion, Wyckoff positions.

#### **Wyckoff Positions**

A crystal structure can be simplified to just a few symmetrically unique positions called Wyckoff positions. These crystallographic positions are significant in that each of the sites described by a Wyckoff position have the same atomic environment, meaning that the properties

(coordination, occupancy, and bonding) of sites within the crystal are divided along these positions. The ideal sublattice model would define a sublattice for each Wyckoff position containing all of the sites of that Wyckoff position. The result of doing so would be general model which can be applied to any binary/ternary system in which the phase might be found. Additionally, Wyckoff positions are well known for all but the most complicated of phases making it a general approach.

Basing a sublattice model on Wyckoff positions alone doesn't come without fault as this approach can be difficult to practically implement. For phases with relatively few Wyckoff positions the aforementioned approach is ideal, and in many cases has already been implemented. For the C15 laves phase a model based on Wyckoff positions has already been implemented, as will later be discussed. For phases with greater than three Wyckoff positions, as is the case with many TCP phases, this option becomes computationally intensive. Number of parameters needed to describe models with additional sublattices or additional components scales exponentially. A sublattice model containing 5 sublattices for a ternary system would contain 243 parameters. It becomes quite apparent that for developing multicomponent thermodynamic databases that additional assumptions will need to be made. At the very least a sublattice model should consider the Wyckoff positions. It is also worth noting that there are circumstances when modeling magnetic properties and ordering that Wyckoff positions too become insufficient for completely describing the system.

### **Coordination Number**

The first assumption that should be made in simplifying sublattice models in cases where the Wyckoff positions lead to computationally intractable results is that based on the

coordination. This method has long been used, and in fact Kasper rules say that sites fill with an arbitrary component in order of coordination. Notation most often used for designating components for describing the order in which they fill sites is to call the component with larger atomic radius A and smaller radius B. Sites with the same coordination are said to fill with component A/B at the same rate and can therefore be combined into the same sublattice. Larger (and more electropositive) elements go to sites of higher coordination as they contain a higher atomic volume and more atoms available for bonding.

While basing a sublattice model on Wyckoff positions and coordination most often leads to a decent result, there are some pitfalls in this approach. The first is an assumption by some that two coordination numbers are approximately the same. This can be seen in some of the TCP phases where as many as 6 Wyckoff positions and more than three values of coordination are seen. Even further assumptions are often made that A atoms sit on the highest coordination site(s), B on the lowest, and mixing on any in between. This assumption is often made without merit, not based on experimental data, but for convenience. A second pitfall is the additional complications that come with ternary systems. In ternary/multicomponent systems it becomes unclear which components act as “A” and “B” if not both in the above schema. That is to say that there are cases when going between binary systems that an A atom in one system might act as a B atom in another.

## **Experimental Data**

To make the most physically accurate models possible, it is crucial that experiments are used. The pitfalls above are most often made in the absence of experimental data or with limited scope of intended use. The most basic and often most available experimental data are solubility



ranges. As previously stated consideration of solubility has been an important and often one of the primary means of structuring sublattice models historically. Mixing of A and B constituents should occur on a sufficient number of sites such that the entire solubility range is covered. Failure to do so results in a model which cannot reproduce the experimentally observed phase equilibria. In addition it is often prudent to include excess solubility for moving into higher order systems. Sublattice models with solubility considerations alone may incorrectly place all of the solubility on a single sublattice. Additional solubility can always be considered by adding mixing to additional sublattices (based on coordination number) to achieve experimentally observed phase equilibria. In the case where site occupancy data is available, determining how to consider solubility becomes a more trivial task.

Among the best experimental data available for the purposes of formulating sublattice models is site occupancies. The reason for such is because site occupancy data reflects the way in which atoms occupy crystal sites. Site occupancies have historically been determined from Mössbauer spectroscopy, limited to relatively simple TCP phases. Further limitations with the method makes it most applicable to iron containing systems<sup>3</sup>. Luckily for the CALPHAD community more general methods have been developed using synchrotron. A good model for a given phase should be able to reproduce the experimentally observed trends in site occupancy. That is to say there should be as many sublattices as there are trends in site occupancy, modeled as the corresponding Wyckoff position. Site occupancy data can further inform models in determining solubility. Recent data from synchrotron in many systems indicate that solubility is often higher than is currently modeled.

Critical evaluation of the site occupancies produced from CALPHAD models also provides a means of evaluating thermodynamic databases. The site occupancies provide a means

of probing the relative energies of the endmembers contained in the sublattice model. As an empirical rule the site occupancies for sublattices should not intersect. This is to say that a given site will have preference for a given constituent regardless of the systems composition. To further understand this the 2 sublattice case will be considered in the following.

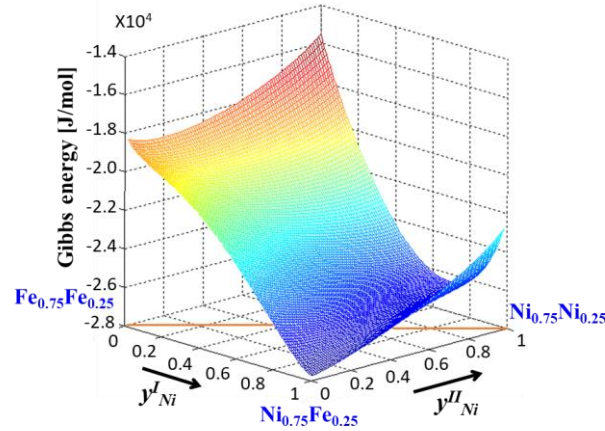


Figure 2-1: Demonstration of Gibb's energy for 2-sublattice system<sup>52</sup>

Trends in site occupancies are determined by the gradient of the Gibbs energy (Figure 2-1) of the system as composition changes between endmembers. This is shown in Figure 2-2 for a general 2 sublattice system. The topology of the Gibbs energy is shown for sublattice Y1 and Y2 with the red curve showing the path the system takes and the dashed line showing where site occupancies between sublattices are equivalent. The corresponding site occupancy vs system composition plot is also shown.

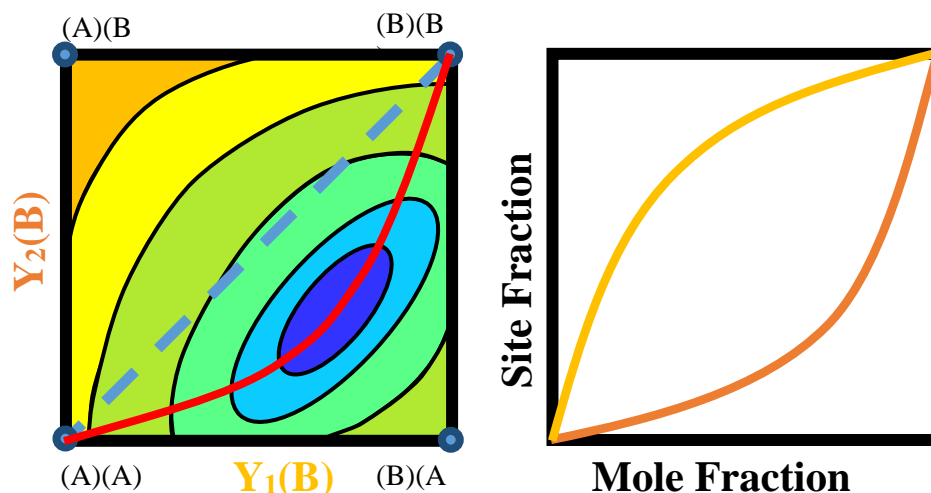


Figure 2-2: Demonstration of topology of the Gibbs free energy in a 2-sublattice system and the corresponding site occupancies.

This is to say that for a given system that there is one endmember that is most energetically favored, often the stoichiometric composition many TCP phases are said to possess, and converge to at low temperatures. Mixing between that endmember and adjacent ones may result in a decrease in energy. Any endmember deviating from this ideal case results in an increase in energy. In order for the sublattice site occupancies to cross the dashed line a complex interaction is necessary, or endmembers must be energetically equivalent. This can be summarized as a sublattice will always have more or less preference for a component regardless of the specific composition, and for trends to cross the affinity for a component would need to change relative to others. In higher dimension systems such as is the case for many of the TCP phases which will hence forth be considered, the chances of endmembers being energetically similar increases, meaning that the accuracy of first principle calculations becomes more significant. Such assessment should be considered in future work as a means of validating endmember energies. Reproducing the site occupancies however doesn't guarantee that the energies relative to the standard element are accurate but only relationships between different configurations for the phase.

For this reason it is important when modeling to include other thermodynamic properties. This has long been the gold standard in CALPHAD modeling. Proper databases use properties related to the Gibbs free energy (Enthalpy/Heat capacity, etc) to fit parameters. Heat capacity is a great choice in fitting thermodynamic databases as its value is not dependent on reference state as are quantities in units of energy (Enthalpy). Inclusion of such data insures that parameters in revised sublattice models are not arbitrarily fit, but represent the real properties of a given structure.

While the inclusion of thermodynamic data is easy to implement for the case of stoichiometric structures where only one equilibrium structure can be found and models don't include solubility (or very limited solubility). Previous discussion in chapter one compared equilibrium to the surface of a lake. In this way it is often impossible to synthesize or sufficiently characterize a given metastable state. The end members on which databases are built are in themselves metastable. In many of the models which will be considered this presents an issue as experimental data is unavailable for fitting parameters of most or all endmembers. First principles calculations (based on density functional theory) provides an attractive solution, providing energetics for a given unit cell of atoms. In later sections methods of practically implementing first principles calculations will be discussed.

### **Physical accuracy vs simplicity and the tradeoff therein**

No conversation about the philosophy and considerations for modeling is complete without discussion of the tradeoff between physical accuracy and simplicity. While it is often convenient and even necessary to put crystal sites in neat boxes called sublattices, the real world often has other plans. Physical phenomena are often complicated, and requires models with

sufficient complexity to represent them. It is for this reason that it is often the choice of the modeler and the availability of resources to decide how much physical accuracy can be captured. In producing CALPHAD models for TCP phases it is impractical to produce large models in high order systems. While first principles can be used to augment gaps in experimental data they too show rather unfavorable scaling for higher order systems. First principles calculations too show tradeoffs between accuracy and computational resources. Use of Debye model over phonon calculations is often necessary in modeling sublattice models of TCP phases, and will be discussed in the methods section. Further supporting calculations and considerations for magnetism can also add to the tradeoff between simplicity and accuracy. All these factors contribute to the choice of sublattice model acting as just as important a criterion as the previously discussed. In some cases this trade off may lead to the necessity for multiple models.

### **Sublattice models in complex solids**

#### **Laves Phases**

Not a single phase but actually a family of phases all with tetrahedral sites shared between A and B components, the laves phases have an ideal stoichiometry of  $AB_2$ , often being called by either their prototype or their Strukturbericht names. The atomic radii of components must satisfy the stoichiometry and near close packing seen in these phases. This provides an ideal ratio of radii of 1.225 between components<sup>4</sup>. In practice there is some deviation from this, but offers a criteria for predicting their formation. The laves phases range from relatively simple crystallography to moderately challenging and as such they are well suited for analysis in this work. The most common Laves phases seen are the C14, C15, and C36 (Strukturbericht designations); each with a different number of sites/Wyckoff positions.

The simplest among these is the C15 laves phase otherwise referred to as the  $\text{MgCu}_2$  phase. The phase contains two Wyckoff positions (see figure 2-3). Wyckoff positions being as few as they are means modeling the phase is reasonable. Databases containing this phase in many cases even contain mixing parameters<sup>5</sup> while the phase in other systems is still modeled as a stoichiometric compound<sup>6,7</sup>. The main issues seen in literature for this phase are less choice of model and more in obtaining accurate stability, as is the case for the Cr-Nb system (see assessments<sup>5,8-11</sup>).

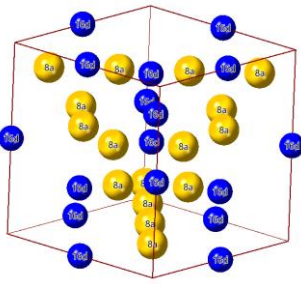
Site	Coordinates	C.N.	Space Group: $\text{Fd}\bar{3}\text{m}(227)$	
8a	(0.125,0.125,0.125)	16	Prototype: $\text{MgCu}_2$	
16d	(0.5,0.5,0.5)	12	Binary systems: Cr-Nb, Cs-Bi, Rb-Bi	

Figure 2-3: Crystallographic information for Laves C15 phase<sup>66,67</sup>

Increasing in complexity is the C14 phase also known by its prototype structure of  $\text{MgZn}_2$ . The C14 phase contains three Wyckoff sites yet is still most often modeled the same as the C15 phase, with a model of  $(\text{A,B})_2(\text{A,B})$ , in the case where extended solubility is considered. The two sublattice model works well for most binary systems, but may present issues when going to higher order systems as previously discussed. Two sublattice models for this system aren't forward compatible and with the relatively manageable number of Wyckoff sites there have been attempts to make models more physically accurate. One such notable attempt has been made in the Fe-Ti binary to model by Hari Kumar<sup>12</sup> where the phase is modeled as  $(\text{B,Va})_2(\text{A,B})_4(\text{B})_6$  with great success. The model implemented by Kumar doesn't include solubility of A (Ti) atoms onto B (Fe) sites because the difference in atomic radii is large and solubility is hypothesized to be more likely achieved through vacancies. Solubility on the iron rich side being provided by vacancies is also supported by literature<sup>13</sup> in the Fe-Yb system, but comes down to the particular

system. Further assessments consider 3 sublattices, such as that in the Fe-Ni-Ti system by Keyzer et al.<sup>14</sup>. However the most recent assessment of the Fe-Ti binary as part of the Fe-Ti-V system the 2 sublattice model is adopted, while claiming to have used the model of their processors with small modifications. This could be in part because vacancies aren't considered in their assessment, opting for the model  $(\text{Fe,Ti,V})_2(\text{Fe,Ti,V})$ .

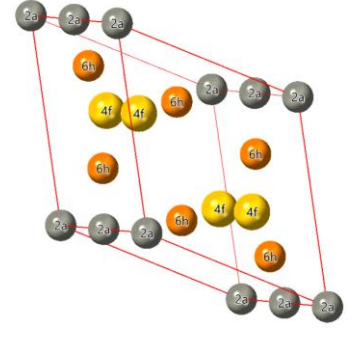
Site	Coordinates	C.N.	Space Group: P6 <sub>3</sub> /mmc(194)	
2a	(0,0,0)	12	Prototype: MgZn <sub>2</sub>	
4f	(0.33,0.66,0.06241)	16	Binary systems: Ca-Mg, Zr-Re, K-Na, Ta-Fe, Nb-Mn, U-Ni, Mg-Zn, Fe-Ti	
6h	(0.17036,0.34072,0.25)	12		

Figure 2-4: Crystallographic information for Laves C14 phase<sup>48</sup>

The C36 laves phase, otherwise referred to by its prototype MgNi<sub>2</sub>, suffers the most of the three phase by the limitation of a two sublattice model as previously discussed in prior phases. The phase contains 5 Wyckoff positions and the unit cell is relatively large with 24 atoms making the 2-sublattice model a significant simplification. The two sublattices in this simplification are made by coordination number. That is to say that the 4e and 4f1 sites are combined on one sublattice and the remaining sites on the other. Despite this it can be seen in a recent assessment of Zr-Cr in the Zr-Nb-Cr system that the two sublattice model was adopted in order to stay consistent in the multicomponent database<sup>11</sup>. In similar fashion to the C14 phase, there have been attempts to add additional sublattices to the C36 phase. The Zr-Cr system has also been modeled as  $(\text{B})_2(\text{A,B})_4(\text{A,B})_6$  by Zeng et al<sup>15,16</sup>. Which is a simplification based on combining the 6g/6h sites as well as 4e/4f on the basis of coordination. Others have proposed modeling the phase in a similar manner<sup>17</sup> where  $(\text{B})_4(\text{A,B})_8(\text{A,B})_{12}$  which is compatible with the one implemented by

Zeng. Reason for treating the low coordination 4f site as exclusively component B in literature is for the sake of simplicity, however the site likely contains some solubility.

Site	Coordinates	C.N.	Space Group: P6 <sub>3</sub> /mmc(194)	
4e	(0,0,0.09373)	16		
4f	(0.33,0.66,0.84417)	16	Prototype: MgNi <sub>2</sub>	
4f	(1/3,2/3,0.12501)	12		
6g	(1/2,0,0)	12	Binary systems: Nb-Zn, Sc-Fe, Th-Mg, Hf-Cr, U-Pt	
6h	(0.16461,0.32922,1/4)	12		

Figure 2-5: Crystallographic information for Laves C36 phase <sup>48</sup>

### $\mu$ Phase

Increasing in complexity from laves phases is the  $\mu$  phase sometimes referred to by its ideal stoichiometry of A<sub>6</sub>B<sub>7</sub>. While the laves phase contains only 2 different interatomic coordination's the  $\mu$  phase contains four (seen in figure 2-6) as well as lower symmetry. The phase contains solubility where B component can occupy A sites as well as the reverse. In fact A atoms in one binary can act as B atoms in another. Such reversal is observed between the Co-W and Co-Nb systems leading to some higher order databases modeling the different stoichiometry as separate phases altogether as pointed out by Jingjun et al.<sup>18</sup>, only further enforcing the need for better sublattice models focused on producing higher order systems. This combined with 5 Wyckoff sites makes selecting a sublattice model unclear. Several different models have been proposed for modeling the  $\mu$  phase and several others have been proposed based on various considerations mentioned in section 2.1.



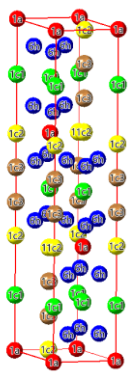
Site	Coordinates	C.N.	Space Group: $R\bar{3}m(166)$	
1a	(0,0,0)	12		
2c1	(0,0,0.167)	16	Prototype: $W_6Fe_7$	
2c2	(0,0,0.346)	15		
2c3	(0,0,0.448)	14	Binary systems: Co-Mo, Co-Nb, Co-Ta, Co-W, Fe-Mo, Fe-Nb, Fe-Ta, Fe-W, Ni-Nb, Ni-Ta, Zn-Ta, Mn-Si	
6h	(0.833,0.166,0.257)	12		

Figure 2-6: Crystallographic information for  $\mu$  phase<sup>68,48</sup>

The first and simplest model is two sublattices  $(A,B)_7(A,B)_6$  where the first contains all low coordination sites (less than 14) and the second containing the remaining sites. As explored in the previous section this is the case where coordination is said to be roughly equal between sites without any justification to do so. The two sublattice model for the mu-phase has been implemented in the Co-Mo system as recently as 2003<sup>19</sup>, however recent assessments for binary systems have included additional sublattices. Ansara also proposes a two sublattice model in his work on modeling TCP phases<sup>17</sup>. Arguments have been made against the 2 sublattice model on the basis of it not covering the homogeneity range, however extended solubility can be considered on both sublattices, and comes down to how well the model can reproduce the physical structure. Additionally, a two sublattice model runs the issue of not covering the relatively flexible stoichiometry of the  $\mu$  phase, only being able to produce  $A_6B_7$  or  $B_6A_7$  endmembers.

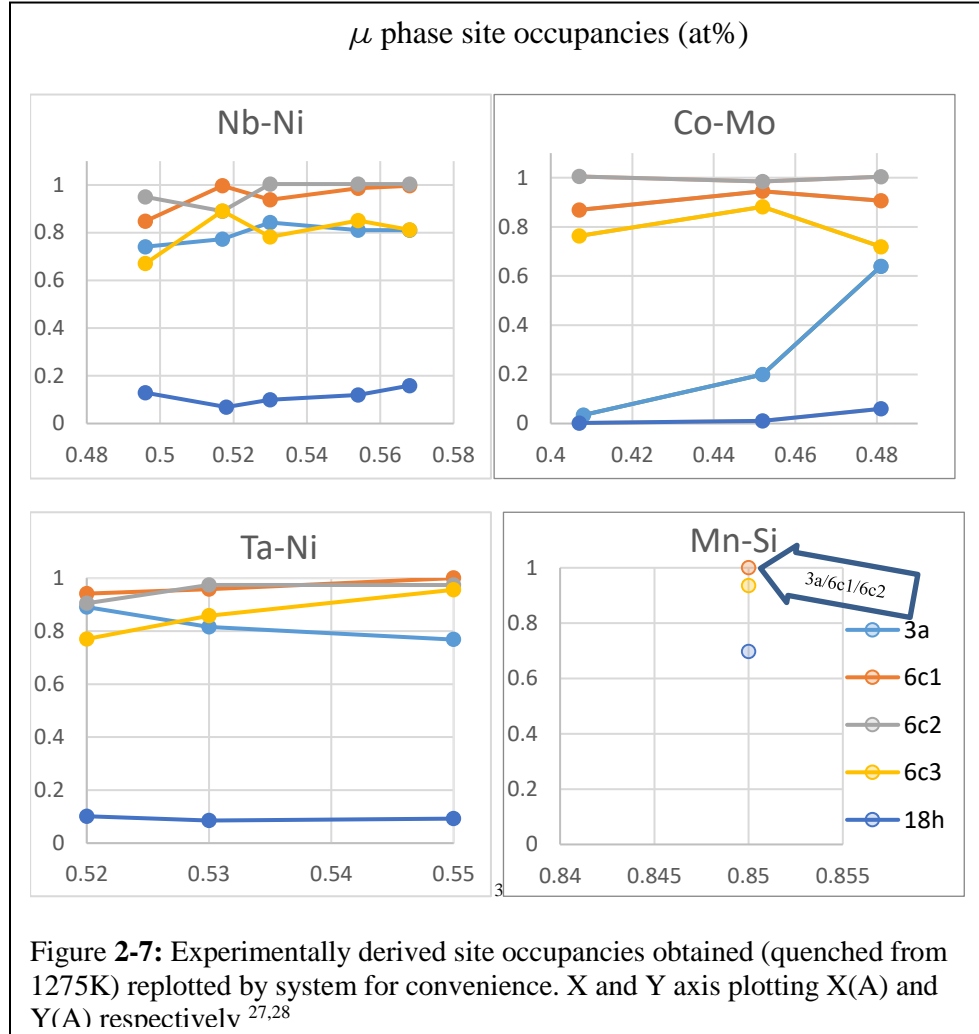
More frequently used models for the  $\mu$  phase contain 3 sublattices generally made under the assumption that sites with coordination of 14 are combined with coordination of 15. This results in a sublattice model of  $(A,B)_4(A)_2(B)_7$ , which only just covers the ideal stoichiometry of 0.538, spanning from 0.538 to 0.846 atomic fraction B<sup>20</sup>. For this reason various assessments have added additional solubility to the A and B containing sublattices so that the model covers the

compositions generally seen for the phase (see **figure 1**). This results in one of the most successfully employed model  $(A,B)_4(A)_2(A,B)_7$  which has been used for the Co-Ta<sup>21</sup>, Co-Nb<sup>22</sup>, and others. The decision to include solubility on the 1a/6h site is generally made on the basis that stoichiometry can flip between elements and on the basis of homogeneity. However there is disagreement on the full homogeneity range encountered in various binary/ternary systems.

It has been recognized that the need to add additional sublattices to the  $\mu$  phase. Several 4 sublattice models have been considered for addressing concerns over homogeneity range. Two in particular are considered by Kumar et al.<sup>22</sup>. The first being  $(A,B)(B)_4(A,B)_2(A)_6$  where 2c1/2c3 sites are combined. Simplicity of modeling is retained by considering mixing on two sublattices. The assumption that these sites will have solubility is reasonable based on coordination, however considering occupation of these sites to be identical may present issues as more experimental data collected. The second model presented,  $(A,B)(B)_2(A,B)_4(A)_6$ , is considered on the basis of increased solubility but later disregarded for its disadvantageous combinatorics. Other models considered elsewhere in literature are similar differing only in how they consider solubility, making them compatible. In at least two recent assessments a 4-sublattice model has been employed, the Co-Nb-W<sup>18</sup> and Co-Ta<sup>23</sup> systems.

In the literature where various sublattice models are considered arguments have been on the basis of coordination or homogeneity range. For many of these assessments, only structural data and phase equilibria were available, with solubility on the 1a site well known<sup>24,25,26</sup>. In 2002 and 2004 a studies were performed using Rietveld refinement of X-ray powder diffraction to determine the experimental site occupations of Ta–Ni, Mo–Co, Mn–Si, and Nb–Ni systems<sup>27,28</sup>. This data has been replotted in figure **2-7** so trends in site occupancy can be seen. Sites contain moderate solubility with the exception of the 6c2 site which is almost exclusively component A (Ta, Mo, Mn, Nb). The 16h sublattice is the primary B containing sublattice and shows a distinct trend in occupancy. The 3a site additionally shows unique occupancy behavior seen in the Co-Mo

system. This would indicate that at least 3 sublattices are needed to describe the phase in the three binaries shown.



### $\chi$ phase

With simpler complexity and a larger unit cell in the  $\chi$ -phase, also referred to as  $\alpha$ -Mn or  $\text{Al}_{12}\text{Mg}_{17}$ . The phase contains the majority of its 58 atoms on 2 of its 4 sublattices (figure 2-8). Information on the phase is relatively limited in large part due to the limited number of systems in

which it forms, the most technologically relevant being in the Mn containing systems and in the Cr-Fe-Mo ternary, occurring in duplex stainless steels.

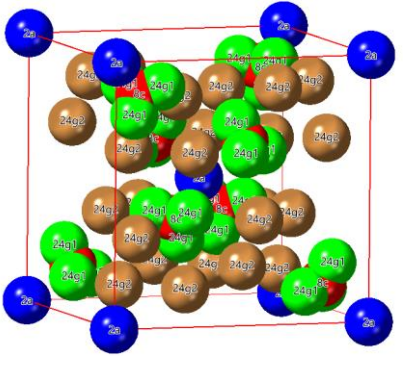
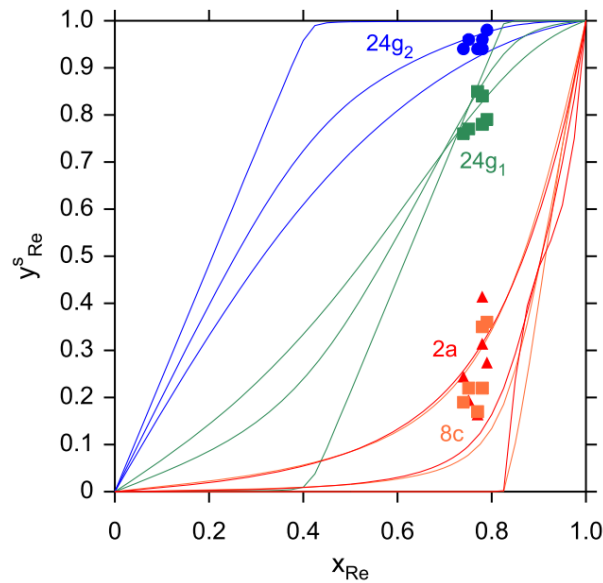
Site	Coordinates	C.N.	Space Group:	
2a	(0,0,0)	16	I4-3m	
8c	(0.636,0.635,0.635)	16	Prototype:	
24g1	(0.392,0.392,0.714)	13	a-Mn, Al <sub>12</sub> Mg <sub>17</sub>	
24g2	(0.372,0.372,0.179)	12	Binary systems: Mo-Re, Cr-Fe-Mo, Al-Mg	

Figure 2-8: Crystallographic information for  $\chi$  phase

In Mn containing systems the phase is generally modeled from SGTE as a single sublattice<sup>29</sup>, treating the phase as a solid solution. This is due in part to the solubility seen in the phase where in the Mn-Fe binary it can accommodate up to 35at% Fe. However as mentioned in the most recent assessment the phase has been observed to have ordering<sup>30</sup>, potentially necessitating the need for more sublattices through an order disorder model.

The most common approach for the phase combines the 2a/8c sites to give a 3-sublattice model which is typically sufficient in binary systems. Despite limited information on the phase experimental site occupancies in the Mo-Re system are available (figure 2-9)<sup>31</sup>. From this three trends in occupancy can be seen among the sites, indicating that 3 sublattices (in the case of the Mo-Re system) are sufficient for modeling the phase. It is also seen that solubility must be considered on all sublattices.



**Figure 2-9:** Site occupancies<sup>64</sup> for the Mo-Re  $\chi$  phase as well as calculated trends from recent assessment<sup>31</sup>

### $\delta$ phase

Yet another intermetallic phase known for its stability in technologically important alloys is the  $\delta$  phase, sometimes referred to as P phase or MoNi. This phase is most prominently known for its occurrence in the Mo-Ni binary, often forming in highly alloyed Nickel alloys. It is for this reason that it is the main intermetallic seen in Ni-based superalloys<sup>32</sup>, causing detriment much like other TCP phases discussed here. The structure of the phase is quite complex in the context of CALPHAD modeling. It contains 14 Wyckoff sites which are always reduced to 4 for the purposes of modeling. Such simplification is made by coordination number<sup>33</sup>. From this considerations of the structure are often further simplified to 3 sublattices on which the coordination 15 and 16 sites are combined. This leaves a sublattice model of

(Ni)<sub>24</sub>(Mo,Ni)<sub>20</sub>(Mo)<sub>12</sub> which is currently in use as of the most recent assessment<sup>34</sup>

retaining the model of its predecessors<sup>35,36,37</sup>.

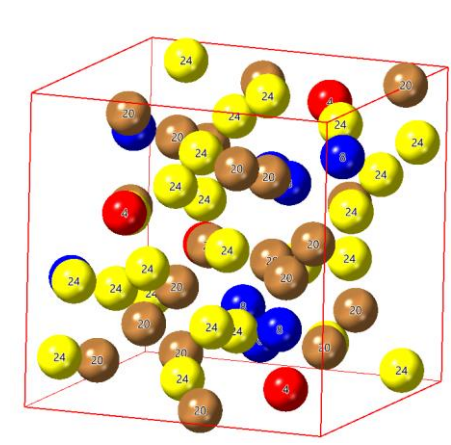
site	Coordinates	C.N.	Space Group:	
24	(0.4519,0.1153,0.5322) (0.4424,0.3662,0.5971) (0.3882,0.0523,0.2748) (0.1337,0.0707,0.2157) (0.3768,0.4358,0.8567) (0.0680, 0.1442,0.9529)	12	P2 <sub>1</sub> 2 <sub>1</sub> 2 <sub>1</sub> (19)	
20	(0.2648,0.1993,0.7486) (0.3136,0.2464,0.0740) (0.0029,0.1969,0.6767) (0.1885,0.0157,0.4960) (0.1031, 0.4192,0.9133)	14	Prototype: NiMo	
8	(0.1763,0.4832,0.6425) (0.0338,0.3398,0.1807)	15	Binary systems:	
4	(0.2289, 0.2865, 0.4098)	16	Ni-Mo	

Figure 2-10: Crystallographic information for Delta-phase<sup>33</sup>

## R-Phase

The R-Phase is an interesting case as it was historically considered to be a ternary compound, and was completely overlooked in binary systems<sup>38</sup>. The phase is seen in ternary systems containing Titanium, Iron, Manganese, and Silicon<sup>39</sup>. Modeling the phase faces similar considerations as the  $\delta$  phase in that it contains 11 Wyckoff sites which must be condensed if there is any chance of modeling it. As a phase that occurs most readily in ternary systems, coupled with relatively low symmetry makes information on the relatively scarce in literature. With the most in depth studies being in the Fe-Mo system, one of the few binaries in which it is stable. The ideal stoichiometry for the phase is Fe<sub>32</sub>Mo<sub>21</sub>. The most Recent assessment by Rajkumar et al.<sup>40</sup> places the R-phase with a model of (Fe)<sub>32</sub>(Mo)<sub>18</sub>(Fe,Mo)<sub>3</sub> constraining the phase to have relatively limited solubility. The model also fails to consider coordination in constructing sublattices, instead basing it on energetics from first principles making it suited only for

describing low energy states. This is in opposition to models used in previous assessments which divide sublattices differently. In particular a model employed in describing the Fe-Mo-C ternary<sup>41</sup> uses  $(\text{Fe})_{27}(\text{Mo})_{14}(\text{Fe},\text{Mo})_{12}$  in which the coordination 15 and 16 sites are combined, assumed to be occupied entirely by Molybdenum. This model possesses the ability to describe higher solubility than needed to describe Fe-Mo, which may be necessary to describe ternary systems.

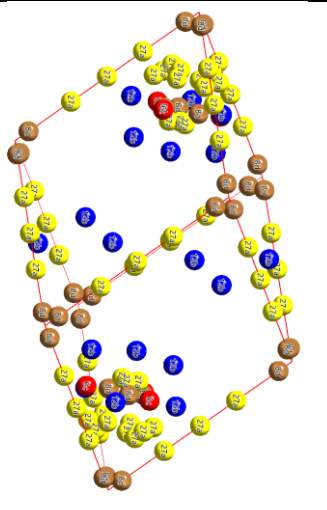
Site	Coordinates	C.N.	Space Group: R-3(148)	
27a	(0,0,0) (0,0,0.1956) (0.2459,0.4197,0.1647) (0.1052,0.3877,0.0667) (0.1393,0.0212,0.3038) (0.1969,0.225,0.2315)	12	Prototype: $\text{Co}_{46}\text{Cr}_{16}\text{Mo}_{38}$	
12b	(0.1265,0.1759,0.1031) (0.2687,0.1132,0.0348)	14	Systems: Fe-Mo, Ti-Mn, Co-Cr-Mo, Co-Mn-Mo, Mo-Mn-Fe, Ti-Mn-Si, Nb-Mn-Si, Ta-Mn-Si, Mo-Mn-Si, W-Mn-Si, V-Ni-Si	
6c	(0.2579,0.033,0.1817)	15		
8d	(0,0,0.4265) (0.1115,0.3996,0.2889)	16		

Figure 2-11: Crystallographic information for R-Phase<sup>69</sup>

### Demonstration of improved model for $\sigma$

As one of the most iconic intermetallic TCP phases, the  $\sigma$  phase is one of the most studied phases and for good reason. Its occurrence can be seen in multiple binaries, often effecting highly alloyed steel. Its structure is sufficiently complex so as to provide a challenge yet sufficiently simple for first principles calculations. As such the  $\sigma$  phase will act as the model phase for the methods discussed in this work. In this way we can explore how first principles and the criteria previously outlined can be procedurally applied to CALPHAD modeling. The Fe-Cr-Ni system will serve as the demonstration of this workflow, necessitating additional considerations for magnetic states among endmembers.

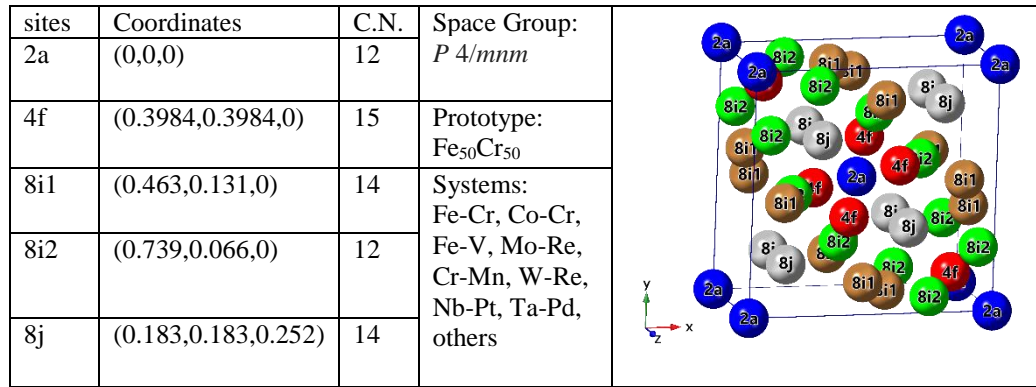


Figure 2-12: Crystallographic information for  $\sigma$  Phase<sup>69</sup>

Several different sublattice models have been successfully employed for the  $\sigma$  phase. Incompatibility between these various models has previously been an impediment to building higher order databases, and ultimately comes down to decision between maintaining compatibility or increasing physical accuracy. The most common among these models in use at the time of publication is the 10-4-16 model in which sites are combined based on coordination number of the given site. In this description the 2a and 8i2 sites are combined (C.N. 12) and the 8i1 and 8j sites (C.N. 14) are combined<sup>42,43</sup>. Historically the 4f site is modeled with exclusively B(Cr) occupation<sup>17</sup> and to a lesser extent the 2a/8i2 as being exclusively A(Fe). Other sublattice models exist with even less physical accuracy including the 10-20 model where coordination (C.N. >12) of the 4f and 8i1/8j sites are considered to be the same<sup>44</sup>. Yet another model, the 8-4-18 model contains even less physical accuracy and as such has fallen out of favor for the aforementioned models<sup>43</sup>. Due to high solubility of  $\sigma$  phase there have been great strides to add solubility to multiple sublattices<sup>45</sup>. In the most recent assessment of the  $\sigma$  phase by Jacob et al.<sup>46</sup> the (Cr,Fe)<sub>10</sub>(Cr,Fe)<sub>4</sub>(Cr,Fe)<sub>16</sub> model was adopted as it more accurately includes solubility on all sublattices. Further attempts outside of the Fe-Cr binary have also been made to include additional physical accuracy.



While including solubility is a vast improvement in modeling the  $\sigma$  phase it still fails to capture the experimental trends in site occupancies. The issue being that 3-sublattice models don't contain enough degrees of freedom, even if solubility is considered on each sublattice. The major limitation of previous models has been in their ability to describe the site occupancies on each Wyckoff position. From figure 4-3 it is observed that the site occupancies from experimental data follow at the very least 4 separate trends. It is also clear that the common assumption that the 4f site can be modeled as purely chrome is not valid, and in fact all of the sites contain high solubility, unable to be considered purely A or B. In addition, the most recent assessment of the Fe-Cr  $\sigma$  phase fails to capture the correct behavior with the 4f, over predicting the solubility of iron. Additionally, the 2a/8i2 sites under predict the solubility of iron.

Recently the Co-Cr  $\sigma$  phase has been modeled based on the Wyckoff positions, which is to say with 5 sublattices<sup>47</sup>. This shows promise as a physically accurate model demonstrating the extraordinary computational power that is available to today's researchers. Site occupancy plots generated with this model appear reasonable but the authors fail to compare this plot to experimental data, most likely because it isn't available in literature. It is for this reason that the current work will implement a 5-sublattice model physically based on the Wyckoff positions. This model will then be extended into ternary Fe-Ni-Cr system including solubility on each sublattice. Due to the large amount of information required about metastable states in the  $\sigma$  phase, it is necessary that first principle calculations be employed to find finite temperature properties.

## Chapter 3

### Methods

#### High throughput DFT with DFTTK

##### Overview

Density Functional Theory, often affectionately referred to with a host of other atomistic techniques as first principles, has become an increasingly powerful tool for producing CALPHAD databases. It provides a means for filling gaps between experiments, and in many cases provides results more quickly than can be achieved experimentally. DFT however has more than the ability to just fill in between missing experiments, allowing researchers exacting control over a system, with the ability to individually control atoms. This allows for the calculation of formation energy of stable and unstable structures alike. With ever growing accuracy of DFT software and power of computational resources it is becoming more feasible to generate thermodynamic databases from first principles alone. To do this however robust workflows must be developed, incorporating domain knowledge, so that structures might stand a chance of being calculated in a high throughput manor.

It is with this spirit that the work presented in the following chapter outlines a procedure for a robust workflow for the calculation of finite temperature properties from DFT. This workflow was built using Atomate software for building and managing first principles calculations. The Atomate software provides a means for adding structures from Materials Project<sup>48</sup> as well as from files or crystallographic data. Atomate software boast the ability to create and run complex material science calculations through relatively easy statements. It is built in python utilizing pymatgen, custodian, and FireWorks libraries making it easy to modify and scale for high

throughput calculations as are seen here. Atomate includes standard workflows which can be used to get various properties. Additional tools are provided for managing and storing results in databases, and using databases for cloud computing. Ease of use, and management tools are of particular interest to this work for building robust workflows for DFTTK. Functionality for building and managing workflows is maintained from Atomate software. The general workflow for finite temperature calculations is detailed below.

An overview of the workflow can be found in **Figure 3-1** and will be referred to in the following sections. In the naming convention in use by Atomate the workflow consist of firetasks (not shown) joined together to create fireworks, usually in the form of a VASP calculation, which are joined to make a workflow. Multiple workflows can be created programmatically enabling high throughput calculations.

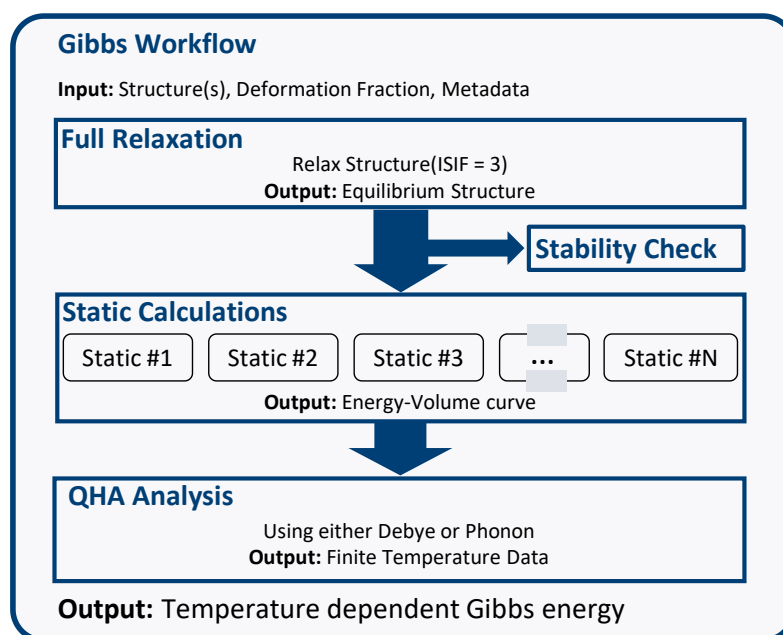


**Figure 3-1:** Outline of developed Work flow built into software termed Density Function theory Tool Kit (DFTTK)

It is here once again stressed that there are always tradeoffs even in the creation of computational workflows, much in the same way that was discussed in the context of CALPHAD databases. Two main tradeoffs must be balanced, the first being attention to detail and capacity.

The larger the number of structures in need of calculation the less attention to detail a researcher can achieve. Finding a balance in this relies on domain knowledge for robustness providing much needed validation in multiple steps of the workflow. The second and possibly more general issue is the tradeoff between accuracy and speed. While domain knowledge provides a solution to the previous trade off it offers no solution for directly increasing accuracy in many cases. The work flow outlined here attempts to balance this in the most reasonable way possible.

Density Functional Theory Tool Kit (DFTTK) calculates all energies from first principles calculations through Vienna Ab-initio Simulation Package (VASP). Generalized Gradient Approximation (GGA) implemented by Perdew, Burke, and Ernzerhof (PBE)<sup>14</sup> was assumed for the exchange-correlation. Projector augmented-wave (PAW) method<sup>15</sup> is used in this work to describe electron-ion interactions with vasp recommended PAW\_PBE pseudopotentials which are best suited for work in alloys, more specifically cr\_pv, fe, and ni was used in this work.

## **Relaxation**

Endmembers are first fully relaxed in volume, cell shape, and ionic positions simultaneously (isif=3) to find the equilibrium structure. To insure the accuracy of these calculations and insure compatibility with Materials Project database an energy cut-off of 520 is used as default. Furthermore to insure accuracy, DFTTK supplies kpoints to vasp with results in a kpoint grid density of 8000 ([5,5,9] in the case of  $\sigma$  phase). Elements displaying magnetism are set to ferromagnetic by default. Magnetic moments may also be supplied as a site property in calculation allowing any configuration to be investigated. Choice of configurations is outside of the scope of the workflow. The magnetic moments of the  $\sigma$  phase as it applies to metastability will be discussed in later chapters.

## E-V Curve

An energy-volume (E-V) curve is then constructed from the given number of deformations and deformation fractions supplied upon calling the workflow. In calculating the  $\sigma$  phase 7 volumes spanning  $\pm 7\%$  the equilibrium volume were used in constructing the E-V curve. For each deformation, static calculations using the tetrahedral method and Blöch corrections<sup>16</sup> are performed. DFT calculations yield the electronic structure and quantities related to the Helmholtz energy for a given atomic structure under given volume  $V$  and temperature  $T$ <sup>17,18</sup>.

$$F(V, T) = E_c(V) + F_{vib}(V, T) + F_{el}(V, T) \quad (1)$$

Where  $E_c(V)$  is the energy predicted at 0 K directly from DFT (i.e. VASP) without contribution from zero-point vibrational energy.  $F_{vib}(V, T)$  is the lattice vibrational free energy which can be calculated from either the Debye model or phonon calculations, and  $F_{el}(V, T)$  the thermal electronic contribution can be evaluated from the electronic densities of state. The thermal electronic contribution to the Helmholtz energy is estimated based on the electronic density of states (DOS) in terms of the Fermi–Dirac statistics for metallic systems<sup>18</sup>. It should be noted that in the case where pressure effects are ignored, the Helmholtz energy can be equated to Gibbs energy.

It should be noted here that calculations of TCP phases which exhibit magnetism present an additional challenge of metastability. There remains the possibility at each point in the E-V curve that magnetism could be that for a metastable state. This results in one or more points in the curve being higher in energy than that of equilibrium, which can be seen as a jump in the curve. Additional issues can arise at smaller volumes where magnetism can drop significantly to small

values causing a similar jump. Recent endeavors into improving the code have provided a means of preventing this (discussed in 3.1.5), but at the time of calculation these improvements have not been incorporated.

### Debye Model

Vibrational contributions to the Helmholtz free energy ( $F_{vib}$ ) can be found through either phonon calculations or Debye model. The workflow supports either of these options, and can be accomplished by providing a phonon supercell matrix and setting the phonon parameter to true. In this work use of the Debye model was necessitated by the large number of structures (endmembers) used to describe the phase, and as such will be detailed below. Vinet Equation of State (EOS) using 4 parameters was fit to the E-V curve<sup>19,20</sup>. The formulation for the EOS was as follows:

$$E(V) = a - \frac{4B_0V_0}{(B'_0 - 1)^2} \left\{ 1 - \frac{3}{2}(B'_0 - 1) \left[ 1 - \left( \frac{V}{V_0} \right)^{\frac{1}{3}} \right] \right\} \exp \left\{ \frac{3}{2}(B'_0 - 1) \left[ 1 - \left( \frac{V}{V_0} \right)^{\frac{1}{3}} \right] \right\} \quad (2)$$

Here  $B_0$  and  $B'_0$  are fitting parameters, and  $V_0$  is the equilibrium volume. There is a subtle difference to the way in which DFTTK treats this fitting to the EOS which may differ from other softwares. The software imposes the limitation that information regarding the EOS is only known for values within bounds set by the calculated E-V curve. This may in instances lead to insufficient information when reaching higher temperatures. Here once again implementation of improvements is planned and detailed in section 3.1.5. The following formulation for the Debye model was used to obtain finite temperature properties<sup>18</sup>:

$$F_{vib}(V, T) = \frac{9}{8}k_B\theta_D(V) - k_B T \left\{ D\left(\frac{\theta_D(V)}{T}\right) + 3\ln\left(1 - e^{-\frac{\theta_D(V)}{T}}\right) \right\} \quad (3)$$

Where  $T$  is temperature,  $K_B$  is Boltzmann's constant,  $D$  the Debye function, and  $\theta_D(V)$  the Debye temperature given as:

$$\theta_D(V) = \frac{\hbar}{k_B} (6\pi^2)^{\frac{1}{3}} f(\sigma) \left(\frac{V}{n}\right)^{-\frac{1}{6}} \left(\frac{B_0}{M}\right)^{\frac{1}{2}} \left(\frac{V_0}{V}\right)^\gamma \quad (4)$$

Where  $B_0$  the bulk modulus,  $V_0$  the equilibrium volume,  $M$  the atomic mass, and  $\gamma$  is the Debye-Gruneisen parameter which is determined from the fitting parameters of the fit EOS. The scaling factor  $f(\sigma)$  is as follows:

$$f(\sigma) = \left[ \frac{2}{3} \left( \left( \frac{2}{3} \frac{1+v}{1-2v} \right)^{\frac{3}{2}} + \left( \frac{1}{3} \frac{1+v}{1-v} \right)^{\frac{3}{2}} \right) \right]^{-\frac{1}{3}} \quad (5)$$

The Poisson ratio( $v$ ) of 0.25 was selected for the Debye model fitting due to the brittle nature of the  $\sigma$  phase. While this quantity can be obtained from first principles, the necessary calculations require a significant amount of computational resources.

### Checking and validation steps

At the present there is a single main validation step implemented into the code with another e to be added to the workflow. The first is a symmetry check on the relaxed structure. Comparing it to the input structure. In order to accomplish this code from the Alloy Theoretic Automated

Toolkit (ATAT)<sup>49</sup> was incorporated. More specifically the Check relax feature which returns a value for the amount of relaxation a structure has undergone. Offending structures which fall above the cutoff are then handled through the use of inflection detection<sup>50</sup>.

Inflection detection provides a means for defining the energetics of mechanically unstable phases by finding the inflection point in the energy when relaxing a structure. Failure to do so may yield a relaxed structure which is approaching a mechanically stable phase rather than the one being calculated. It is therefore the energy of the inflection point which is taken to be the relaxed structure<sup>50</sup>. Full discussion on inflection detection is important for understanding the energetics of mechanically unstable phases but is outside the scope of this work.

There are currently additional plans to add a validation step after calculation of the E-V curve. As was mentioned before, there are occasions, especially when working in magnetic systems where calculation of points along the E-V curve will fail to yield the equilibrium structure. In these cases a point will be above the E-V curve resulting in a poor fit of the EOS. To combat this an algorithm is proposed in which points with large error relative to the EOS fit are excluded and an adjacent volume calculated. This can be procedurally run a number of times to produce E-V curves with a better fit, or in the event of a failure to produce a better fit exclude the point from the fitting altogether. Another check may be included by running the Debye model to insure deformations are sufficiently spaced from the equilibrium volume so as to insure the fit EOS produces results at higher temperature. This is necessitated by the fact that DFTTK imposes boundary conditions on the EOS fitting set by the largest deformations. In this way the majority of issues in calculating finite temperature properties of TCP phases exhibiting magnetism are solved.



## High throughput CALPHAD modeling ESPEI

### Overview of Software and Capabilities

Thermodynamic modeling of the Cr-Fe-Ni system, through use of optimization software in the spirit of the CALPHAD methodology, was built on pure element data adopted from the SGTE database<sup>51</sup>. The phase description used in this work for  $\Sigma$  phase is  $(\text{Cr,Fe,Ni})_2(\text{Cr,Fe,Ni})_4(\text{Cr,Fe,Ni})_8(\text{Cr,Fe,Ni})_8(\text{Cr,Fe,Ni})_8$ . The Gibbs energy for a 5 sublattice model of the  $\sigma$  phase can be written as follows:

$$G_m = \sum_i \sum_j \sum_k \sum_l \sum_m y_i^{2a} y_j^{4f} y_k^{8i1} y_l^{8i2} y_m^{8j} G_{i:j:k:l:m} - TS_m \quad (6)$$

Here i,j,k,l,m are indices containing the elements for the ternary system (Cr,Fe,Ni), and y is the site occupancy of a particular sublattice.  $G_{i:j:k:l:m}$  is the Gibbs energy of a particular endmember with the configuration given by the indices.  $S_m$  is the molar entropy. Due to the number or degrees of freedom due to endmembers no mixing parameters were used in this model.

### Selection of model parameters

Creation of model parameters was done through Extensible Self-optimizing Phase Equilibria Infrastructure (ESPEI) software, an open source tool made for fitting and optimizing parameters in the CALPHAD method. Derivatives of the Gibbs energy, either from experiments or first principles<sup>52</sup>, are used to parameterize the Gibbs energy of each phase individually in the compound energy formalism (CEF). The form of fit parameters take the following:

$$G = a + bT + cT^2 + dT^3 + eT\ln(T) \quad (7)$$

ESPEI fits single phase data to create phase descriptions, in this case for the  $\sigma$  phase. Enthalpy, Entropy, and Heat capacity data from previously mentioned first principles calculations are used for parameter selection. It is important to note that all of the values used for parameter selection including heat capacity are referenced to the pure element data. This is done so as to minimize any systematic error that might be introduced from first principles calculations.

### Optimization to phase equilibria

Upon generation of parameters data was then added to the last major assessment of the Cr-Fe-Ni ternary<sup>53</sup>. As is typical for solution phases, generated parameters were optimized to phase equilibria data. ESPEI also provides a means for doing this through the use of Markov Chain Monte Carlo (MCMC). Zero phase fraction data was taken from literature and used for optimization<sup>42,54–57</sup>. Once again due to size and complexity of the model, which potentially contains in excess of 1000 variables of which to fit, it was not feasible to fit every degree of freedom independently. Instead an offset and composition term were collectively introduced to all parameters in the  $\sigma$  phase giving model parameters the functional form of:

$$G = a + bT + cT^2 + dT^3 + eT\ln(T) + OFFSET + y_{Fe}XSFE \quad (8)$$

The offset term which takes the form of  $A+BT$  reduces the degrees of freedom to just two variables enabling the use of MCMC functionality from ESPEI. The introduction of this offset term does not change the relationship between endmembers, as it is assumed that any discrepancies from first principles data is systematic in nature and not dependent on composition.

The compositional term was added taking the form of CT adding an additional degree of freedom to the model. This added term allows for a better match to phase equilibria data and to account for any compositionally depended discrepancies that are present in first principles results. First order temperature terms were selected because the Debye model often fails to accurately predict entropy. First order terms offer a constant change in entropy, which is the first derivative of Gibbs energy.

## Chapter 4

### Analysis

#### DFT calculations for $\sigma$ phase

In calculating the  $\sigma$  phase it was found that the pure Fe  $\sigma$  endmember was 10 kJ/mol atom more stable than previously reported. Upon investigating this, it was found that previous attempts in calculating this endmember and likely others may have only calculated a metastable state, and therefore not found the most relaxed structure. Attempts to replicate this were made by constraining the magnetic moments. This is demonstrated in **Figure 4-1** by changing the “NUPDOWN” setting within VASP which holds the total magnetization constant while performing volume relaxations. It can be seen the result from the current work falls along the minima of this curve indicating that the equilibrium magnetization was found.

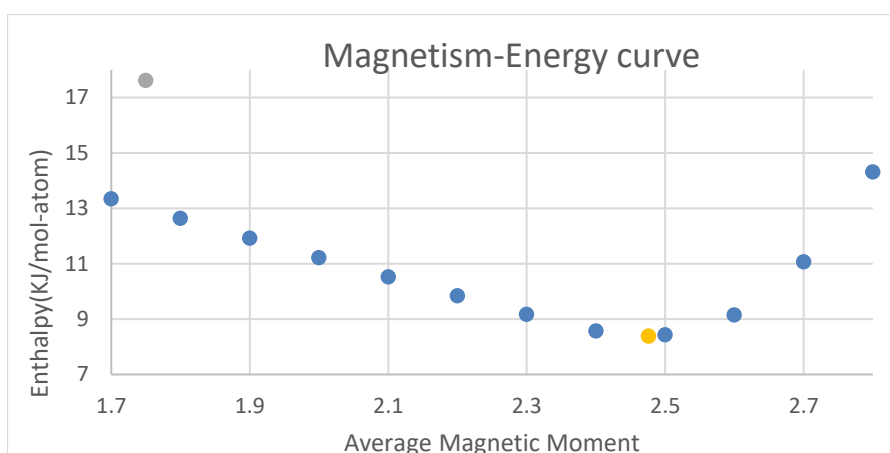


Figure 4-1: Plotted in blue average magnetic moment vs energy found through volume relaxations only. Orange is equilibrium structure and in Gray from Pavlu<sup>29</sup>

The average magnetic moment per atom is similar to that of BCC iron at just under 2.5. Without the ability to individually constrain the magnetic moments it is impossible to replicate previous results, however when the total magnetic moment for the cell is held to the same value reported by Pavlu et al.<sup>58</sup> it is observed in Table 4-1 that the individual magnetic moments for each Wyckoff position are similar in value. Looking at a brief overview of other endmembers we see similar trends in relative stability as is observed from Pavlu.

Table 4-1: Comparing the magnetic moments from Pavlu et al.<sup>58</sup> and magnetic moments in the current work when total magnetic moment is held at the same value

	2a	4f	8i1	8i2	8j	Avg
Pavlu	1.10	2.29	2.00	1.22	1.87	1.75
C.W.	0.84	2.38	2.01	1.03	1.92	1.70

The current body of work includes Ab initio calculations for all 243 endmembers in the Cr-Fe-Ni system, with many of the less stable ternary endmembers having been calculated for the first time. A complete summary of these results can be found in supplementary materials as well

as in a dataset hosted by Citrine<sup>59</sup>. The binary endmembers for the Cr-Fe and a comparison of results from literature are presented in Table **4-2**. It is clear from literature results that there is some disagreement in the formation energies for endmembers for  $\sigma$  phase. Such discrepancies between results are likely due to the propensity for large structures with magnetism to find local minima when relaxed, leading to metastable states. Pure element endmembers (also shown in Table **4-2**) of the  $\sigma$  phase have been calculated and compared with the literature. While nonmagnetic endmembers match well with literature there is some discrepancy in the pure Fe/Ni endmembers.

Table 4-2: Fe-Cr end members compared with literature

\*non-magnetic structure

X(Cr)	Element/Magnetic moment					Lattice Constants		Energy	
	2a	4f	8i1	8i2	8j	a	c	Current Work	Literature
0	Fe/1.56	Fe/2.56	Fe/2.31	Fe/1.98	Fe/2.25	8.592	4.511	7.423/25.571*	17.6 <sup>70</sup> /17.647 <sup>58</sup> /25.777 <sup>58</sup> *
0.07	<b>Cr/-1.73</b>	Fe/2.4	Fe/2.34	Fe/1.91	Fe/2.16	8.620	4.541	6.801	16.2304667 <sup>58</sup>
0.13	Fe/0.64	<b>Cr/-1.1</b>	Fe/2.05	Fe/1.5	Fe/1.83	8.471	4.488	7.322	14.5989333 <sup>58</sup> /15.27 <sup>46</sup>
0.2	<b>Cr/-0.69</b>	<b>Cr/-0.78</b>	Fe/2.0	Fe/1.19	Fe/1.74	8.441	4.491	8.937	14.7404 <sup>58</sup>
0.27	Fe/1.79	Fe/2.16	<b>Cr/-1.04</b>	Fe/1.18	Fe/1.9	8.620	4.517	10.05	<b>12.3428667</b> <sup>58</sup>
0.27	Fe/1.04	Fe/2.12	Fe/1.81	<b>Cr/-1.12</b>	Fe/1.84	8.545	4.497	8.659	<b>13.6278667</b> <sup>58</sup>
0.27	Fe/1.28	Fe/2.26	Fe/1.97	Fe/1.36	<b>Cr/-0.67</b>	8.642	4.527	8.837	<b>12.3618667</b> <sup>58</sup>
0.33	<b>Cr/-0.79</b>	Fe/1.8	<b>Cr/-0.68</b>	Fe/0.83	Fe/1.73	8.503	4.468	6.473	11.3723333 <sup>58</sup>
0.33	<b>Cr/0.14</b>	Fe/1.75	Fe/1.73	<b>Cr/-0.81</b>	Fe/1.71	8.484	4.468	10.417	14.9353333 <sup>58</sup> /14.89 <sup>46</sup>
0.33	<b>Cr/-0.26</b>	Fe/1.87	Fe/1.57	Fe/0.82	<b>Cr/-0.4</b>	8.446	4.421	8.823	---
0.4	Fe/-0.42	<b>Cr/0.2</b>	<b>Cr/-0.12</b>	Fe/0.17	Fe/1.39	8.393	4.383	8.596	11.8938 <sup>58</sup>
0.4	Fe/0.29	<b>Cr/0.2</b>	Fe/-0.78	<b>Cr/0.03</b>	Fe/1.39	8.438	4.440	10.917	13.4388 <sup>58</sup>
0.47	<b>Cr/0.11</b>	<b>Cr/-0.05</b>	Fe/0.97	Fe/0.64	<b>Cr/-0.19</b>	8.446	4.409	10.040	11.8932667 <sup>58</sup>
0.47	<b>Cr/-0.16</b>	<b>Cr/0.14</b>	Fe/-1.03	<b>Cr/0.12</b>	Fe/1.32	8.461	4.476	13.340	14.6862667 <sup>58</sup> /12.35 <sup>46</sup>
0.47	<b>Cr/-0.32</b>	<b>Cr/0.28</b>	<b>Cr/-0.19</b>	Fe/0.35	Fe/1.38	8.398	4.420	8.701	11.4282667 <sup>58</sup>
0.53	Fe/0.97	Fe/1.73	<b>Cr/-0.11</b>	<b>Cr/-0.24</b>	Fe/1.54	8.512	4.523	12.582	15.0587333 <sup>58</sup>
0.53	Fe/0.09	Fe/-0.29	<b>Cr/0.03</b>	Fe/-0.02	<b>Cr/0.01</b>	8.443	4.322	6.912	10.5867333 <sup>58</sup> / 4.62 <sup>46</sup>
0.53	Fe/0.11	Fe/1.83	Fe/1.32	<b>Cr/-0.2</b>	<b>Cr/-0.09</b>	8.488	4.421	10.735	12.9557333 <sup>58</sup>
0.6	<b>Cr/-0.02</b>	Fe/1.78	Fe/1.32	<b>Cr/-0.17</b>	<b>Cr/-0.09</b>	8.489	4.455	13.044	14.2452 <sup>58</sup>
0.6	<b>Cr/-0.02</b>	Fe/-0.39	<b>Cr/0.03</b>	Fe/-0.09	<b>Cr/0.02</b>	8.457	4.353	8.026	10.7022 <sup>58</sup>
0.6	<b>Cr/-0.08</b>	Fe/-0.84	<b>Cr/0.04</b>	<b>Cr/-0.15</b>	Fe/1.22	8.455	4.491	15.129	16.2182 <sup>58</sup>
0.67	Fe/0.17	<b>Cr/0.15</b>	Fe/-1.0	<b>Cr/0.22</b>	<b>Cr/-0.01</b>	8.508	4.410	11.055	12.4726667 <sup>58</sup>
0.67	Fe/-0.01	<b>Cr/0.0</b>	<b>Cr/-0.0</b>	Fe/0.0	<b>Cr/0.0</b>	8.487	4.345	4.864	8.3486667 <sup>58</sup> /5.62 <sup>46</sup>
0.67	Fe/0.12	<b>Cr/0.2</b>	<b>Cr/-0.0</b>	<b>Cr/-0.14</b>	Fe/1.39	8.516	4.521	12.904	14.1716667 <sup>58</sup>
0.73	<b>Cr/-0.04</b>	<b>Cr/0.07</b>	Fe/-0.99	<b>Cr/0.15</b>	<b>Cr/0.03</b>	8.516	4.444	11.998	13.6821333 <sup>58</sup>
0.73	<b>Cr/0.01</b>	<b>Cr/0.01</b>	<b>Cr/-0.0</b>	Fe/0.01	<b>Cr/-0.0</b>	8.506	4.368	5.871	9.26213333 <sup>58</sup>
0.73	<b>Cr/-0.1</b>	<b>Cr/0.23</b>	<b>Cr/-0.02</b>	<b>Cr/-0.04</b>	Fe/1.25	8.452	4.508	13.635	15.1301333 <sup>58</sup>
0.8	Fe/-0.0	Fe/-0.06	<b>Cr/0.0</b>	<b>Cr/-0.0</b>	<b>Cr/0.0</b>	8.548	4.453	15.745	14.9986 <sup>58</sup>
0.87	<b>Cr/0.02</b>	Fe/-0.25	<b>Cr/0.02</b>	<b>Cr/-0.03</b>	<b>Cr/-0.01</b>	8.517	4.468	18.277	16.2450667 <sup>58</sup> /14.11 <sup>46</sup>
0.93	Fe/0.01	<b>Cr/0.01</b>	<b>Cr/-0.0</b>	<b>Cr/0.0</b>	<b>Cr/0.0</b>	8.643	4.477	11.285	12.6585333 <sup>58</sup>
1	<b>Cr/-0.0</b>	<b>Cr/-0.0</b>	<b>Cr/-0.0</b>	<b>Cr/0.0</b>	<b>Cr/-0.0</b>	8.571	4.482	13.708	12.20 <sup>71</sup> /13.394 <sup>58</sup> /13.2 <sup>70</sup>
---	Ni/0.56	Ni/0.54	Ni/0.57	Ni/0.59	Ni/0.56	8.367	4.451	9.474	8.71 <sup>71</sup> /16.5 <sup>70</sup>

As discussed previously the Debye model was used in this work due to the volume of calculations considered. In the following we will evaluate the finite temperature properties so as to assess the ability of the Debye model to capture the thermodynamics of TCP phases. The most critical of the properties for this type of assessment are the heat capacities. Heat capacity is an ideal quantity as it is common in literature and does not require a reference state like quantities related to the energy of the system. In looking at the data between various endmembers (hosted on Citrine Informatics) it is seen that all endmembers are practically identical in heat capacity value at low temperature. A comparison between experimental data<sup>60</sup> and the most stable endmember at similar composition in figure 4-2. In addition the weighted pure element  $\sigma$  endmembers are shown. Disagreement can be seen between first principle calculations with reasonable Poisson ratio and experimental data. Because the temperatures below 1000K are primarily controlled by Poisson ratio exploration of this value is shown. While a value of 4.5 gives good agreement with experimental data, it is unreasonable for a brittle phase such as  $\sigma$  (and most TCP phases).

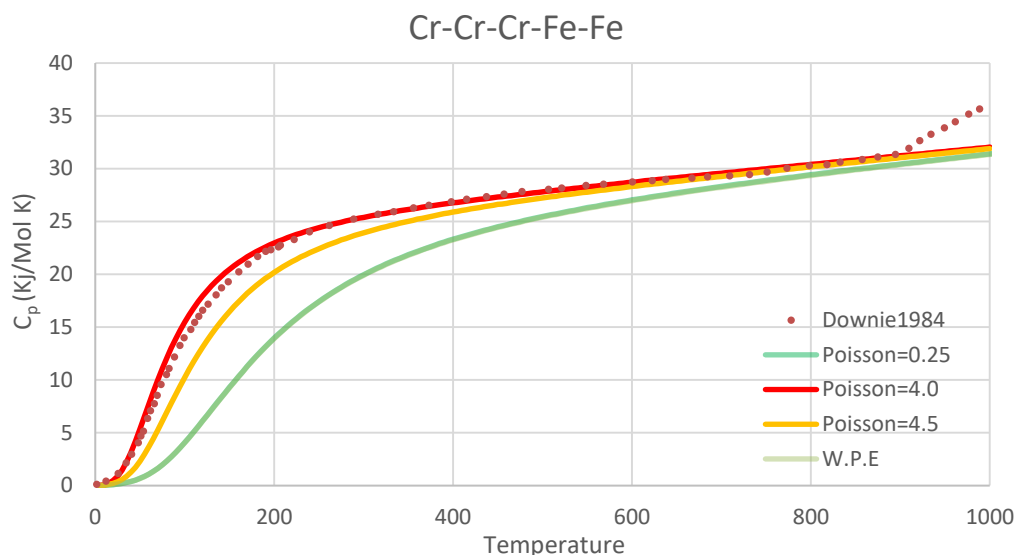


Figure 4-2: Above shown the effect of changing Poisson ratio of heat capacity in comparison to Downie 1984<sup>60</sup>. Weighted pure element  $\sigma$  structures shown averaged (W.P.E)

It was for this reason that this endmember was further investigated through use of elastic calculations to compute the Poisson ratio. The results are shown in **Table 4-3**, and can be summarized as showing the Poisson ratio to be 0.278, far closer to the assumed value than what would satisfy experiments. At the present time a full explanation isn't available for the discrepancy in heat capacity data, however the Debye model may be limited in its ability to describe the heat capacity and should be exercised with this in mind. Luckily multiple options exist, one of which is to use phonon calculations which may give better results. Yet another option is to assume all compositions behave similarly to the experimental data available at given composition. This is reasonable as first principles data shows similar low temperature behavior for all endmembers. Yet another way to proceed to exclude heat capacity data from parameter generation. In the work presented here first principles heat capacity data is included for consistency as well as demonstration of the method.



**Table 4-3:** Summary of elastic calculation results

Comparison of Poisson ratios		
Structure	Calc.	Lit.
Cr-Cr-Cr-Fe-Fe	0.278	-----
Bcc-Fe	0.296	0.32
Bcc-Cr	0.296	0.29

### Creation of the $\sigma$ phase thermodynamic database

Upon completion of first principles calculations analysis, including how to proceed with discrepancies in the heat capacity, quantities were parameterized. From this a thermodynamic phase description was constructed in the manor detailed in the methods section (3.2.2) the site occupancies were plotted. As previously mentioned the major limitation of previous models has been in their ability to describe the site occupancies on each Wyckoff position. The most recent assessment of the  $\sigma$  phase fails to capture the correct behavior with the 4f, over predicting the solubility of iron. Additionally, the 2a/8i2 sites under predict the solubility of iron.

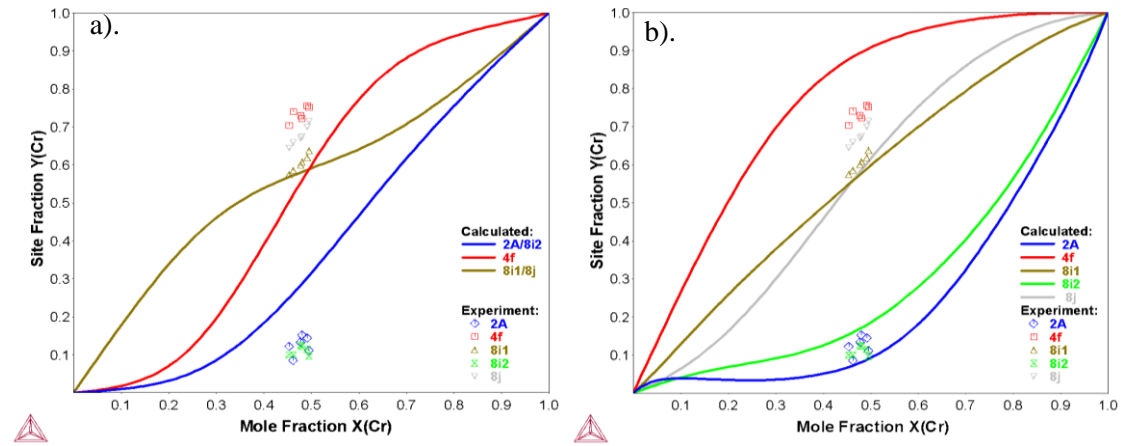


Figure 4-3: Site occupancies for Fe-Cr from most a.) recent assessment<sup>72</sup>, and b.) the present work with experimental data<sup>73,74</sup>

The current model also shown in **Figure 4-3** is able to much better predict the solubility of the 2a and 8i2 sites, and more closely resembles the trends in experimental occupancy of the other 3 sublattices. In addition site occupancy data can be predicted for much more than the Fe-Cr

binary and in fact can be predicted for any composition in the ternary. Site occupancies for Fe-Ni cannot be calculated from previous phase descriptions as the 4f sublattice contains neither Fe nor Ni in its' description. For compositions outside of what is stable such as in the Fe-Ni and Cr-Ni (**Figure 4-4**) binaries there is no experimental data to compare to however the site occupancies are reasonable and match the trends in energy seen from first principle calculations. It should also be noted that other ternary databases may not generate the plots presented in Figure 18 sublattices exist which contain neither element. As mentioned in our criteria the site occupancies offer a diagnostic. It should be noted that the site occupancies shown in **Figure 4-3** are seen crossing between sublattices, in the previous description from Pavlů et al, and in the current description. This is likely due to metastable states caused by magnetism or limitations of DFT.

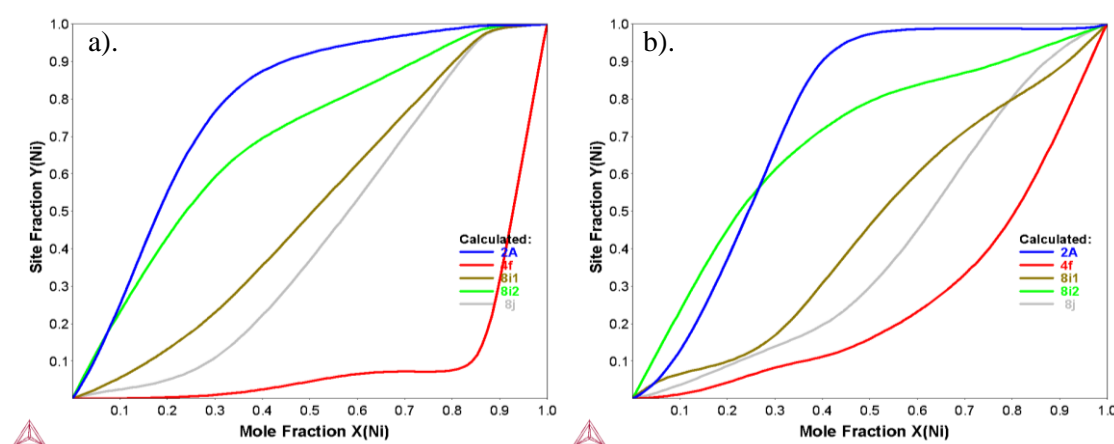
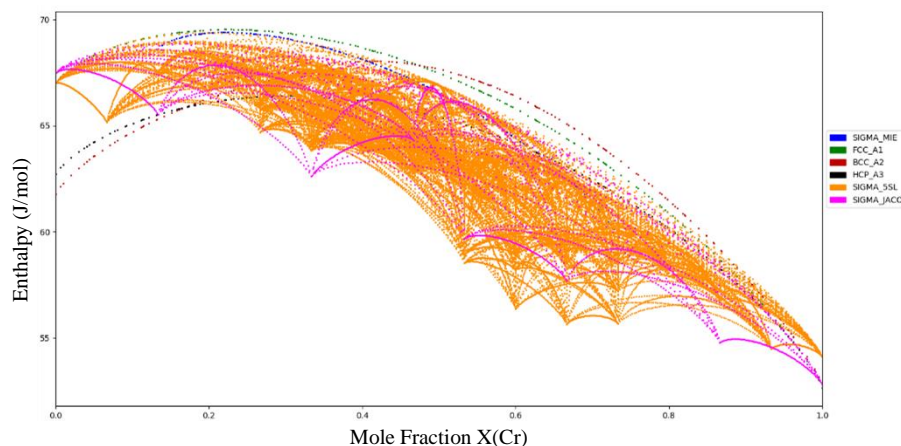


Figure 4-4: Site occupancies for a.) Cr-Ni, and b.) Fe-Ni from current work

This initial phase description was then added to an open source database for the ternary system more specifically that of Miettinen<sup>53</sup>. Parameters for the  $\sigma$  phase were then optimized with ESPEI in the method previously outlined. Parameters were fit to experimental data<sup>44,54,61,62</sup> through the universal offset/compositionally dependent terms so that the energetics of the system can be adjusted uniformly. It would be incorrect in this case to modify individual values in this case as it may over fit the system. Which is where a model requires more/unnecessary parameters

than are available to describe the data which is available for the system. The offset and compositional terms are meant only to correct for systematic differences which maybe present from DFT. It is important for fitting parameters to be structured as such for two reasons. The first being that modification of these parameters does not modify the site occupancies, which is to say that the energetic relationships between endmembers are not altered. Altering these relationships could be of detriment as experimental data present is only available from first principle calculations and site occupancies, and not determined by phase equilibria. Additional reason for structuring fitting parameters in this way come from an effort not to provide too many degrees of freedom for fitting. If for example a second compositional term were to be added; the value of these terms may ‘wonder’ while still maintaining the ability to provide the same energetics. It is for this reason that fitting parameters should be selected such that they aren’t directly dependent on each other’s values.



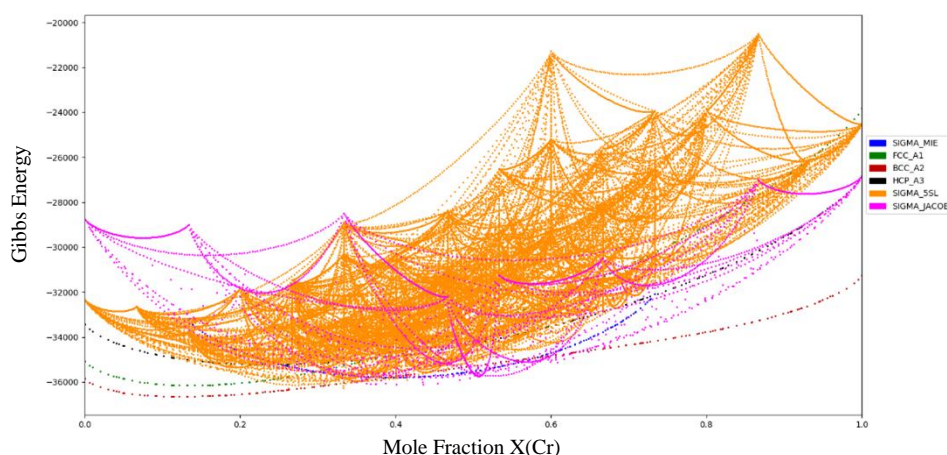


Figure 4-5: comparison of a.)Entropy, and b.)Gibbs Energy between current work and previous phase descriptions

In order to further assess the quality of the first principles data and of the optimized database parameters it is necessary to compare the thermodynamic properties of the 5-sublattice model with that of previous assessments. The properties for the Cr-Fe binary are shown in Figure 4-5, and have been calculated from PYCALPHAD open source software. In models where mixing takes place over multiple sublattices, there are potentially many internal degrees of freedom present, which presents an issue when assessing and creating databases. It can become difficult to determine which if any parameter is an outlier in a database where only the convex hull is calculated. In PYCALPHAD this is solved by showing each endmember as well as the mixing between them producing an envelope of energies and further providing insight into the energetics of the system. This is invaluable as a diagnostic tool in assessing databases as it shows which if any endmembers are outliers such that they can be further investigated and rectified. Entropy for the phase matches well with previous assessments falling between previous assessments. Finally, the phase diagram for the Fe-Cr binary is shown in figure 4-6 with experimental data used for optimization plotted. The majority of the phase equilibria data comes from Cook<sup>54</sup>, past that data in literature available in literature is more sparse. Decent agreement

has been reached for the invariant reaction for which data from De nys<sup>63</sup> and Hertzman<sup>42</sup> is most relevant. The homogeneity region does show some disagreement relative to the other phase boundaries, however this is consistent with previous assessments. The shape of the single phase region is discussed by Jacob<sup>46</sup>.

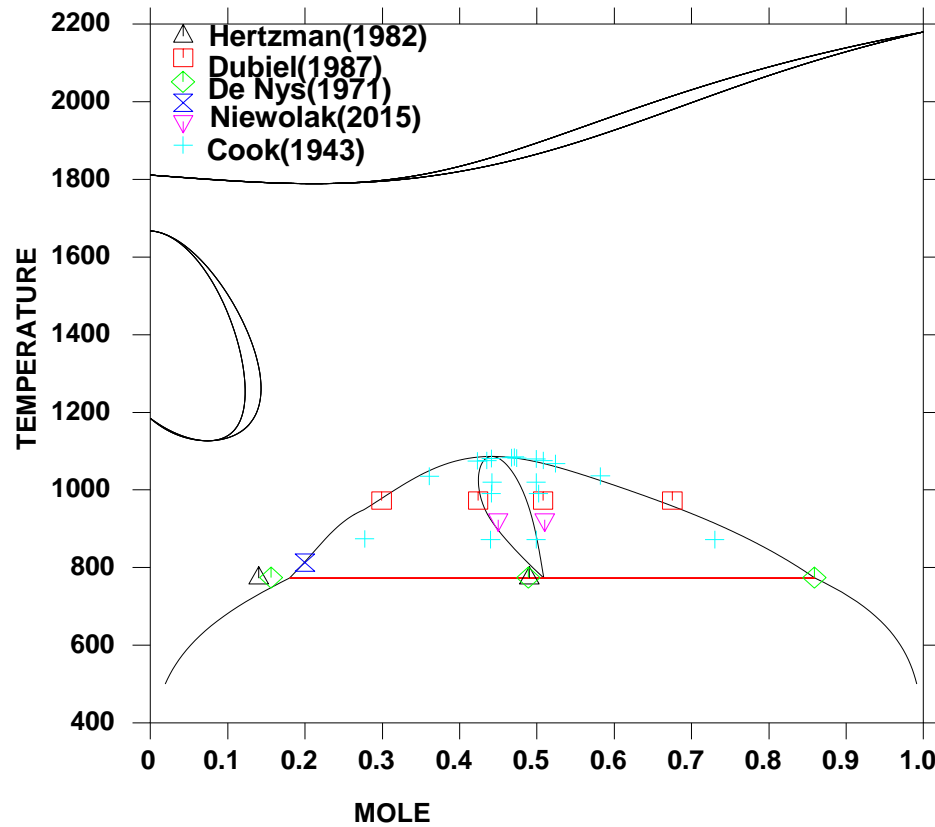


Figure 4-6: Optimized  $\sigma$  phase in Fe-Cr binary phase diagram with experimental data plotted<sup>42,54-56,63</sup>

## Chapter 5

### Discussion

#### Sublattice models in other phases

As previously discussed the goal of this work is not only to demonstrate the method for selection and creation of physically accurate sublattice model, but also to propose such models

for TCP phases. In this work phases considered were the laves C15/C14/C36,  $\mu$ ,  $\chi$ ,  $\delta$ , R, and  $\sigma$  phases. In the following chapter the previously reviewed crystallographic and experimental data relevant to the criteria set forward will be critically reviewed and an ideal model proposed. Where needed several models may be proposed for the tradeoff of convenience vs physical accuracy. The models proposed will also account for increased solubility which is often found from site occupancy data. Solubility on some sublattices may not be necessary for a particular binary/ternary system but is included here to be as general as possible.

For the laves C15 phase only 2 Wyckoff sites are present making choice of model trivial. The ideal sublattice model is (A,B)<sub>2</sub>(A,B) which is also ideal for multicomponent systems. With a relatively simple sublattice model it is tractable to compute mixing between sublattices (SQS/Dilute) to give more fidelity. Moving up in complexity is the C14 phase where 3 Wyckoff sites are present. Modeling still remain relatively simple for 3-sublattices, and being based on the Wyckoff sites, is forward compatible for multicomponent systems. This is in spite of a recent assessment abandoning the 3-sublattice model in favor of the 2-sublattice. The ideal model for C14 laves phase should take the form (A/Va,B)<sub>2</sub>(A,B)<sub>4</sub>(A,B)<sub>6</sub>. It should also be noted that in several cases vacancies (shown as Va) have also been modeled, and comes down to experimental observation in the particular system. For the C36 laves phase 5 Wyckoff sites are present making choice of sublattice model less obvious. Based on the criteria set forth simplification based on coordination leaves a three sublattice model of (B)<sub>2</sub>(A,B)<sub>4</sub>(A,B)<sub>6</sub><sup>15,16</sup> or (B)<sub>4</sub>(A,B)<sub>8</sub>(A,B)<sub>12</sub><sup>17</sup>. Both of which are compatible with each other and can be used interchangeably by adjusting the energy to be per mole atom. These models are ideal in binary systems, but caution should be exercised in multicomponent systems, especially where experimental data might show this simplification not suitable. Finally, the success of 2 sublattices for the sigma phase can't be denied and is often applicable because of the large difference in atomic radii seen in systems in

which they form. In many cases for binary systems it may be suitable to use this model, but should be avoided for forward compatibility.

For the Mu phase which has increased complexity yet it is less clear to select an ideal sublattice model, with 5 Wyckoff positions present. This has led to the adoption of several sublattice models of 2, 3, and 4 sublattices. Most often either based on the ideal stoichiometry, or on the homogeneity range. In CALPHAD modeling homogeneity range is not as significant as in stated in many older assessments, this is due to the ability to add increased solubility to accommodate any homogeneity range possible. It is for this reason that the physical accuracy should lead choice of model. In looking over experimental data for site occupancy we can observe trends and make a determination of how the model should be structured. Looking at Co-Mo the 3a site changes significantly in occupation constituting the majority of the solubility in that system. In addition the 18h site contains the majority of the B type constituent. In addition the 6c3 shows some difference in its trend for occupation most noticeable in the Ta-Ni system. The remaining site account for the A constituent and show similar trends. It is with this in mind that a model (3a)3(18h)18(6c3)6(6c1/6c2)12 seems most accurate. This is compatible with the model determined in assessments of the co-nb-w<sup>18</sup> and co-ta<sup>23</sup> systems, and can be used interchangeably in the same way seen in laves C36. It has the advantage of being based on coordination number (combining the highest occupancy sites). Solubility should be considered on the 18h sublattice in the case of the Mn-Si system as it shows high solubility but may be less necessary in other systems. Solubility considerations for each sublattice may vary in a particular system. As more data is collected in the Mn-Si system is likely that the same trends will be observed as in the previous 3.

Posing a different challenge than the mu phase, the chi phase has a larger unit cell with 58 atoms. As previously discussed the phase has large solubility as shown in **Figure 1**, making

solubility the main concern in modeling. In review of the experimental site occupancies<sup>64</sup> for the Mo-Re system trends between the 4 Wyckoff positions can be observed. That is mainly that there are three distinct trends in occupation. The 2a/8c sites have the same solubility characteristics, leading to the conclusion that the (A,B)10(A,B)24(B)24 model can be used. It is likely that in other binary/ternary systems solubility must be considered on the 24g2 site, with solubility already implemented in the most recent assessment<sup>31</sup>. Further site occupancy data would be ideal to confirm the continued success of this model. Utilization of this model is most needed in manganese containing systems where alpha manganese is modeled from SGTE as a single sublattice.

Modeling in the  $\delta$  phase is simple relative to some of the other TCP phases discussed. Considering each of the 14 Wyckoff sites is challenging and costly in terms of resources such that simplification based on coordination number is all but required. Choice in modeling is also benefited in that the phase is primarily seen in the Mo-Ni binary system, extending into proceeding ternary systems. In other phases a wide number of constituents need be considered and the choice of model must reflect this, but in the  $\delta$  phase only Mo-Ni need be considered. For this reason the existing sublattice model, (A)24(A,B)20(B)12, is likely sufficient with one caveat. This is that extended solubility may need to be considered on A/B sublattices in future assessments which extend into multicomponent systems.

Possessing similar options in modeling to the  $\delta$  phase, the R-phase contains 11 Wyckoff sites all of which are combined based on coordination number into 4 potential sublattices. Experimental site occupancies are not available for the system at the time of writing. For this reason the (Fe)<sub>27</sub>(Mo)<sub>14</sub>(Fe,Mo)<sub>12</sub> model is sufficient, but should be used with caution as the phase is most often seen in ternary systems having historically being overlooked entirely in binary systems. Future experiments and assessments may show it necessary that the 4 sublattice model be used, (A,B)27,(A,B)8(A,B)6(A,B)12, as solubility of sublattices is often higher than



previous established. Additionally models based on first principles energies alone should be used with caution, as metastability is observed for structures as complex as TCP phases, especially those exhibiting magnetic properties (such as Fe-Mo). Such models should always be used in cooperation with experimental results and not as a replacement.

**Table 5-1:** Summary of more physically accurate sublattice models

Phase	Model
Laves C15	$(A,B)_2(A,B)$
Laves C14	$(A/Va,B)_2(A,B)_4(A,B)_6$
Laves C36	$(B)_2(A,B)_4(A,B)_6$ $(B)_4(A,B)_8(A,B)_{12}$
Mu	$(A,B)_3(A,B)_6(A)_{12}(A,B)_{18}$
X	$(A,B)_{10}(A,B)_{24}(A,B)_{24}$
Delta	$(A)_{24}(A,B)_{20}(B)_{12}$
R	$(A)_{27}(B)_{14}(A,B)_{12}$ $(A,B)_{27}(A,B)_8(A,B)_6(A,B)_{12}$

## Chapter 6

### Conclusion

The work presented here aims to serve as a guide for future efforts in modeling TCP phases in the CALPHAD method. Included in this guide is a method for selecting more physically accurate sublattice models in which several criteria were identified in contributing greatly to the crystallography of a phase. These criteria are Wyckoff positions, coordination number and experimental data of which site occupancies are particularly useful. Arguments based off of homogeneity range were also considered. With these criteria in hand, sublattice models for several of the most popular and often challenging TCP phases were critically reviewed and inspected for these criteria. These

phases included several laves phases (C14, C15, C36),  $\mu$ ,  $\chi$ ,  $\delta$ , R, and  $\sigma$  phases. In the preceding chapters the  $\sigma$  phase, one of the most iconic TCP phases was assessed and modeled for a ternary system of great technological importance (Fe-Cr-Ni). This included the use of high throughput software for first principles calculations, and thermodynamic modeling software. Energetics and thermodynamic properties are compared with recent descriptions of the phase. Finally the ideal models for the TCP phases considered were proposed so that future efforts in modeling these phases are compatible as the community pushes for the development of multicomponent databases.

This work includes several deliverables which are of importance for the CALPHAD community. Work on modeling the  $\sigma$  phase has resulted in large amounts of data produced. Such first principles data along with accompanying finite temperature calculations can be found on citrination<sup>59</sup>, and efforts are already underway to use this amassed data for machine learning so that the enthalpy of formation might be predicted in the future. This data can also be of use in producing any given sublattice model for the  $\sigma$  phase, and can be used to produce the common 3 sublattice models (10-4-16/8-4-18). In addition the TDB file which has been optimized for the Fe-Cr-Ni  $\sigma$  phase is available and will be included in a publication (date journal TBA). Additionally, DFTTK, the software developed for performing high throughput first principles calculations is available on github, and can be downloaded and modified. Additionally ESPEI software can also be found on github. It is the hope of the author that these tools, along with updated  $\sigma$  phase data and revised sublattice models may contribute toward the community and aid future CALPHAD modeling.

## References

1. Frank, F. C. & Kasper, J. S. Complex alloy structures regarded as sphere packings. I. Definitions and basic principles. *Acta Crystallogr.* **11**, 184–190 (1958).
2. Pohl, M., Storz, O. & Glogowski, T. Effect of intermetallic precipitations on the properties of duplex stainless steel. *Mater. Charact.* **58**, 65–71 (2007).
3. Zem, T. MOssbauer spectroscopy and structural analysis of solids. 26–31 (1994).
4. Pearson, W. B. Laves structures,  $MgCu_2$ ,  $MgZn_2$ ,  $MgNi_2$ . *Acta Crystallogr. Sect. B Struct. Crystallogr. Cryst. Chem.* **24**, 7–9 (1968).
5. Jiang, Y., Zomorodpoosh, S., Roslyakova, I. & Zhang, L. Calphad Thermodynamic re-assessment of binary Cr-Nb system down to 0 K. *Calphad* **62**, 109–118 (2018).
6. Djaballah, Y. *et al.* CALPHAD : Computer Coupling of Phase Diagrams and Thermochemistry Thermodynamic description of the Bi – Cs and Bi – Tm system supported by first-principles calculations. **48**, 72–78 (2015).
7. Liu, M., Li, C., Du, Z., Guo, C. & Niu, C. Thermochimica Acta Thermodynamic assessment of the Bi – Rb binary system. *Thermochim. Acta* **551**, 27–32 (2013).
8. Pavlů, J., Vřešť, J. & Šob, M. CALPHAD : Computer Coupling of Phase Diagrams and Thermochemistry Re-modeling of Laves phases in the Cr – Nb and Cr – Ta systems using first-principles results. *CALPHAD Comput. Coupling Phase Diagrams* \penalty \z@ \protect \futurelet \@let@token *Thermochem.* **33**, 179–186 (2009).
9. Neto, J. G. C., Fries, S. G. & Lukas, H. L. THERMODYNAMIC of the Nb-Cr SYSTEM. **17**, 219–228 (1993).
10. Hallstedt, B., Markus, T., Schmetterer, C. & Khvan, A. A New Theoretical Study of the Cr-Nb System. **35**, 434–444 (2014).
11. Lu, H. *et al.* CALPHAD : Computer Coupling of Phase Diagrams and Thermochemistry Thermodynamic modeling of Cr – Nb and Zr – Cr with extension to the ternary Zr – Nb –

- Cr system. *Calphad* **50**, 134–143 (2015).
12. K.C. Han' Kumar. P. Wollants, and L. D. IWASSESSMENTAND CALCULATION Fe-Ti PHASE DIAGRAM OF. *Calphad* **18**, 223–234 (1994).
  13. Vereshchagin, L. F. NEW PHASES MELT QUENCHED UNDER HIGH PRESSURE R-Fe SYSTEMS (R = Pr, Sm, Dy, Tb, Ho, Er, Tm, Yb, Lu). **108**, 115–121 (1985).
  14. Keyzer, J. De, Cacciamani, G., Dupin, N. & Wollants, P. CALPHAD : Computer Coupling of Phase Diagrams and Thermochemistry Thermodynamic modeling and optimization of the Fe – Ni – Ti system. *CALPHAD Comput. Coupling Phase Diagrams* **33**, 109–123 (2009).
  15. Kejun, Z., Hamalainen, M. & Lilius, K. Thermodynamic modeling of the laves phase in the Cr-Zr system. **17**, 101–107 (1993).
  16. Kejun, Z., Hamalainen, M. & Luoma, R. A thermodynamic assesment of the Cr-Zr system. *Zeischrift Fur Met.* **84**, 23–28 (1993).
  17. Ansara, I. *et al.* Thermodynamic modelling of selected topologically close-packed intermetallic compounds. *Calphad* **21**, 171–218 (1997).
  18. Xingjun, L., Zeming, N., Yong, L. & Jiajia, H. Thermodynamic Assessment of Co-Nb-W System. *Rare Met. Mater. Eng.* **47**, 2919–2926 (2018).
  19. V., K. A. & R., D. U. Revised Thermodynamic Description for the Co-Mo System. *J. Phase Equilibria* **24**, 209–211 (2003).
  20. Guillermet, A. F. The Fe–Mo (Iron–Molybdenum) system. *Bull. Alloy Phase Diagrams* **3**, 359–367 (1982).
  21. Chang, Y. A. & Zi-Kui Liu. Thermodynamic assesment of the Co-Ta system. *CALPHAD* **23**, 339–356 (2000).
  22. Kumar, K. C. H., Ansara, I. & Wollants, P. Sublattice modelling of the  $\mu$ -phase. *Calphad* **22**, 323–334 (1998).

23. Wang, P. *et al.* Calphad Thermodynamic assessment of the Co-Ta system. *Calphad* **64**, 205–212 (2019).
24. Kripyakevitch PI, Gladyshevskii EI, S. R. No Title. *Sov Phys— Crystallogr* **12**, 525–527 (1968).
25. Kripyakevitch PI, Gladyshevskii EI, P. E. No Title. *Sov Phys— Crystallogr* **7**, 165–168 (1962).
26. Wagner V, Conrad M, H. B. No Title. *Acta Crystallogr. C* **51**, 1241–1243 (1995).
27. Joubert, J. M. & Dupin, N. Mixed site occupancies in the  $\mu$  phase. *Intermetallics* **12**, 1373–1380 (2004).
28. Joubert, J. M. & Feutelais, Y. Contribution of the Rietveld Method to Non-Stoichiometric Phase Modeling. Part II:  $\gamma$ -Ti<sub>3</sub>TeJ and  $\mu$  Nb-Ni as experimental examples. *Calphad* **26**, 427–438 (2002).
29. Bigdeli, S. & Selleby, M. A thermodynamic assessment of the binary Fe-Mn system for the third generation of Calphad databases. *Calphad Comput. Coupling Phase Diagrams Thermochem.* **64**, 185–195 (2019).
30. A. Holden, J.D. Bolton, E. R. P. Structure and properties of iron manfanese alloys. *J. Iron steel Inst.* 271 (1971).
31. Mathieu, R. *et al.* CALPHAD description of the Mo-Re system focused on the sigma phase modeling. *Calphad Comput. Coupling Phase Diagrams Thermochem.* **43**, 18–31 (2013).
32. Shoemaker, L. E. Alloys 625 and 725: Trends in properties and applications. *6th Int. Symp. Superalloys 718, 625, 706 Deriv.* 409–418 (2005).  
doi:10.7449/2005/Superalloys\_2005\_409\_418
33. Shoemaker, C. B. & Shoemaker, D. P. The crystal structure of the  $\delta$  phase Mo-Ni. *Acta Crystallogr.* **16**, 997–1009 (1963).

34. Yaqoob, K., Crivello, J. C. & Joubert, J. M. Thermodynamic modeling of the Mo–Ni system. *Calphad Comput. Coupling Phase Diagrams Thermochem.* **62**, 215–222 (2018).
35. Karin Frisk. A THERMODYNAMIC EVALUATION OF THE Mo-Ni SYSTEM. *Calphad* **14**, 311–320 (1990).
36. Y. Cui, X. Lu, Z. J. Experimental study and thermodynamic assessment of the Ni-Mo-Ta ternary system. *Met. Mater. Trans. A* **30**, 2735–2744 (1999).
37. Zhou, S. H. *et al.* First-principles calculations and thermodynamic modeling of the Ni-Mo system. *Mater. Sci. Eng. A* **397**, 288–296 (2005).
38. von Goldbeck, O. K. *IRON—Binary Phase Diagrams*. (Springer Berlin Heidelberg, 1982). doi:10.1007/978-3-662-08024-5
39. Bardos, D. I., Gupta, K. P. & Beck, P. A. New ternary R-phases with silicon. *Nature* **192**, 744 (1961).
40. Rajkumar, V. B. & Hari Kumar, K. C. Thermodynamic modeling of the Fe-Mo system coupled with experiments and ab initio calculations. *J. Alloys Compd.* **611**, 303–312 (2014).
41. Andersson, J.-O. A thermodynamic evaluation of the Fe–Mo–C system. *Calphad* **12**, 9–23 (1988).
42. Hertzman, S. & Sundman, B. A thermodynamic analysis of the Fe-Cr system. *Calphad* **6**, 67–80 (1982).
43. Sundman, B. Thermodynamic properties of the Cr-Fe system. *Calphad* **11**, 83–92 (1987).
44. Xiong, W. *et al.* An improved thermodynamic modeling of the FeCr system down to zero kelvin coupled with key experiments. *Calphad Comput. Coupling Phase Diagrams Thermochem.* **35**, 355–366 (2011).
45. Chuang, Y. Y. & Austin Chang, Y. A thermodynamic model for ternary sigma phase. *Scr. Metall.* **20**, 1115–1118 (1986).

46. Jacob, A., Povoden-Karadeniz, E. & Kozeschnik, E. Revised thermodynamic description of the Fe-Cr system based on an improved sublattice model of the  $\sigma$  phase. *Calphad Comput. Coupling Phase Diagrams Thermochem.* **60**, 16–28 (2018).
47. Li, Z., Mao, H., Korzhavyi, P. A. & Selleby, M. Thermodynamic reassessment of the Co-Cr system supported by first-principles calculations. *Calphad Comput. Coupling Phase Diagrams Thermochem.* **52**, 1–7 (2016).
48. A. Jain, S.P. Ong, G. Hautier, W. Chen, W.D. Richards, S. Dacek, S. Cholia, D. Gunter, D. Skinner, G. Ceder, K. A. P. The Materials Project: A materials genome approach to accelerating materials innovation. *APL Mater.* **1**, (2013).
49. van de Walle, A., Asta, M. & Ceder, G. The alloy theoretic automated toolkit: A user guide. *Calphad* **26**, 539–553 (2002).
50. van de Walle, A., Sun, R., Hong, Q. J. & Kadkhodaei, S. Software tools for high-throughput CALPHAD from first-principles data. *Calphad Comput. Coupling Phase Diagrams Thermochem.* **58**, 70–81 (2017).
51. Dinsdale, A. T. SGTE DATA FOR PURE ELEMENTS A T Dinsdale Division of Materials Metrology, National Physical Laboratory, Teddington, Middlesex, TW1 1 OLW, UK. *Calphad* **15**, 317–425 (1991).
52. Liu, Z. K. First-principles calculations and CALPHAD modeling of thermodynamics. *J. Phase Equilibria Diffus.* **30**, 517–534 (2009).
53. Miettinen, J. Thermodynamic reassessment of Fe-Cr-Ni system with emphasis on the iron-rich corner. *Calphad Comput. Coupling Phase Diagrams Thermochem.* **23**, 231–248 (1999).
54. J., C. & Jones, F. W. the brittle constituent of the iron-chromium system( $\sigma$  phase). 217–226 (1943).
55. DUBIEL, S. M. & INDEN, G. Miscibility Gap in the Fe-Cr System: A Moessbauer Study

- on Long Term Annealed Alloys. *Int. J. Mater. Res. Adv. Tech.* **78**, 544–549 (1987).
56. Niewolak, L., Garcia-Fresnillo, L., Meier, G. H. & Quadakkers, W. J. Sigma-phase formation in high chromium ferritic steels at 650 °C. *J. Alloys Compd.* **638**, 405–418 (2015).
  57. Novy, S., Pareige, P. & Pareige, C. Atomic scale analysis and phase separation understanding in a thermally aged Fe-20 at.%Cr alloy. *J. Nucl. Mater.* **384**, 96–102 (2009).
  58. Pavlů, J., Vřešťál, J. & Šob, M. Ab initio study of formation energy and magnetism of sigma phase in Cr-Fe and Cr-Co systems. *Intermetallics* **18**, 212–220 (2010).
  59. Feurer, M., Liu, Z.-K., Beese, A., Shang, S. & Brandon Bucklund. Sigma Phase Finite Temperature Calculations. (2019). doi:<https://doi.org/10.25920/YJRC-ZJ59>
  60. Downie, D. B. & Martin, J. F. Heat capacities of transition-metal Fe , ~ ,,, Cr ,,,, alloys and. 143–152 (1984).
  61. Chandra, D. & Schwartz, L. H. Moessbauer effect study of the 475 oC decomposition of iron-chromium. *Metall. Trans.* **2**, 511–519 (1971).
  62. Pomey, G. & Bastien, P. Les transformations des alliages fer-chrome au voisinage de la composition équiatomique. *Rev. Métallurgie* **53**, 147–159 (1956).
  63. NYS, T. DE & M.GIELEN, P. Spinodal decomposition in the Fe-Cr system. *Metall. Trans.* **2**, 1423–1428 (1971).
  64. Farzadfar, S. A., Levesque, M., Phejar, M. & Joubert, J. M. Thermodynamic assessment of the Molybdenum-Rhenium system. *Calphad Comput. Coupling Phase Diagrams Thermochem.* **33**, 502–510 (2009).
  65. Joubert, J.-M. & Crivello, J.-C. Non-Stoichiometry and Calphad Modeling of Frank-Kasper Phases. *Appl. Sci.* **2**, 669–681 (2012).
  66. Mehl, M. J. *et al.* The AFLOW Library of Crystallographic Prototypes: Part 1. *Comput.*



- Mater. Sci.* **136**, S1–S828 (2017).
67. Hicks, D. *et al.* The AFLOW Library of Crystallographic Prototypes: Part 2. *Comput. Mater. Sci.* **161**, (2019).
  68. Cieslak, J., Przewoznik, J. & Dubiel, S. M. Structural and electronic properties of the  $\mu$ -phase Fe-Mo compounds. *J. Alloys Compd.* **612**, 465–470 (2014).
  69. R phase, Mo-Co-Cr (Cr<sub>0.16</sub>Mo<sub>0.38</sub>Co<sub>0.46</sub>) Crystal Structure: Datasheet from ‘PAULING FILE Multinaries Edition – 2012’ in SpringerMaterials ([https://materials.springer.com/isp/crystallographic/docs/sd\\_1252337](https://materials.springer.com/isp/crystallographic/docs/sd_1252337)).
  70. Sluiter, M. H. F. Ab initio lattice stabilities of some elemental complex structures. *Calphad Comput. Coupling Phase Diagrams Thermochem.* **30**, 357–366 (2006).
  71. Palumbo, M., Abe, T., Fries, S. G. & Pasturel, A. First-principles approach to phase stability for a ternary  $\sigma$  phase: Application to Cr-Ni-Re. *Phys. Rev. B - Condens. Matter Mater. Phys.* **83**, 1–2 (2011).
  72. Jacob, calphad 2018.
  73. Yakel, H. L. Atom distributions in sigma phases. I. Fe and Cr atom distributions in a binary sigma phase equilibrated at 1063, 1013 and 923 K. *Acta Crystallogr. Sect. B* **39**, 20–28 (1983).
  74. Cieślak, J., Reissner, M., Dubiel, S. M., Wernisch, J. & Steiner, W. Influence of composition and annealing conditions on the site-occupation in the  $\sigma$ -phase of Fe–Cr and Fe–V systems. *J. Alloys Compd.* **460**, 20–25 (2008).